Solar Energy 302 (2025) 114057

Contents lists available at ScienceDirect

Solar Energy

journal homepage: www.elsevier.com/locate/solener

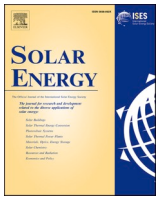

Determination of reflectance of interest from limited state-of-the-art solar reflector field soiling measurements

Johannes Wette [a,*], Florian Sutter [b], Teresa Diamantino [c], Marco Montecchi [d], Gregor Bern [e], Aránzazu Fernández-García [a]

[a] Centro de Investigaciones Energéticas, Medioambientales y Tecnológicas (CIEMAT). Plataforma Solar de Almería (PSA), Ctra. de Senés s/n km 4, Apartado 22, 04200 Tabernas, Spain
[b] German Aerospace Center (DLR), Institute of Solar Research, Calle Doctor Carracido 44, 1st floor, 04005 Almería, Spain
[c] Laboratório Nacional de Energia e Geologia (LNEG). Estrada do Paço do Lumiar, Nº 22, 1649-038 Lisboa, Portugal
[d] ENEA, Via Anguillarese 301, 00123 Santa Maria di Galeria, Roma, Italy
[e] Fraunhofer Institute for Solar Energy Systems ISE, Heidenhofstr. 2, 79110 Freiburg, Germany

ARTICLE INFO

Keywords:
Soiling measurements
Reflectometers
Correlations
Solar reflectors
Concentrated solar thermal technologies

ABSTRACT

In concentrated solar thermal technologies, plant operators usually monitor the soiling of their solar field with handheld reflectometers. These measurements can be used for yield calculations and to adapt cleaning strategies: if the reflectometer reading falls below an empirically established threshold, the solar field should be cleaned. There are several commercial reflectometers available for this purpose, but all of them measure at different combinations of wavelength, acceptance angle or incidence angle. It is the purpose of this study to bring the readings from all main commercial reflectometers to the same representative value, enabling their comparison with one another and the translation of these readings into a meaningful reflectance parameter. Thus, different handheld reflectometers are correlated with a laboratory reflectometer, capable of measuring in the whole solar spectral region, covering a wide range of incidence and acceptance angles. The most significant parameter is the near-specular solar-weighted reflectance, measured at the typical incidence and acceptance angles for a given plant, as it is the most precise parameter to describe the reflected energy from the solar field. The correlations for all included reflectometers, show highly linear correlations over a wide range of soiling levels with low deviations. Consequently, the correlations presented herein enable the plant operators at the studied site to compute the near-specular solar-weighted reflectance from their reflectometer readings. and, with that, increase the significance of the measurements without collecting any additional data. The work also establishes a detailed procedure to derive this type of correlations at any site of interest.

1. Introduction

Concentrating solar thermal (CST) technologies are one of the promising types of solar energy harvesting to tackle the challenge of the decarbonizing of the world's energy system [1]. Even though the worldwide installed capacity of CST is relatively small in comparison to photovoltaics (PV), it is predicted to play an important role in the future energy mix [2,3]. The main advantages that make it a promising candidate lie in its efficiency in providing direct thermal energy and energy storage [4]. In terms of electricity generation, its primary benefits are the potential to provide reliability, flexibility, and auxiliary services such as inertia support and synchronous power generation, due to its use of turbines similar to conventional thermal power plants [5].

In CST systems, reflectors are used to redirect incoming solar irradiation and concentrate it onto a receiver. This receiver then heats up and transfers the thermal energy to a heat transfer fluid (e.g. oil, molten salt, water/steam, air, or solid particles), which increases its enthalpy. One of the challenges here is to perform this conversion process efficiently, minimizing any losses along the process. The reflectors play a crucial role in this mainly for two reasons: firstly, any incoming radiation that is not redirected onto the receiver is lost for the energy conversion; secondly, the reflectors possess a large surface area, as the concentration relies on focusing irradiation from a large to a small area. This makes maintenance (like replacement or cleaning) of the solar field energy-, cost- and labor-intensive. Following this, the main

* Corresponding author.
E-mail address: johannes.wette@psa.es (J. Wette).

https://doi.org/10.1016/j.solener.2025.114057
Received 27 June 2025; Received in revised form 27 August 2025; Accepted 8 October 2025
Available online 16 October 2025

Nomenclature

Symbols

θ_i	Incidence angle [°]
λ	Wavelength [nm]
ρ	Reflectance [-]
$\rho_{s,\varphi}$	Solar-weighted near-normal near-specular reflectance [-]
$\rho_{\lambda,\varphi}$	Spectral near-normal near-specular reflectance [-]
ρ_{clean}	Reflectance in clean state [-]
ρ_{soiled}	Reflectance in soiled state [-]
φ	Acceptance (half) angle [mrad]
ξ	Cleanliness [-]
a	Slope of linear equation
b	Y-axis intercept of linear equation
%pt	Percentage points
*	the use of [-] implies dimensionless quantities

Acronyms

CIEMAT	*Centro de Investigaciones Energéticas, Medioambientales y Tecnológicas*
CRS	Central receiver system
CST	Concentrating solar thermal
O&M	Operation and maintenance
PSA	Plataforma Solar de Almería
PTC	Parabolic-trough collector
PV	Photovoltaic
S2R	Laboratory Spectral Specular Reflectometer
COI	Site specific cleanliness of interest
ROI	Site specific reflectance of interest

requirements for solar reflectors are high reflectance and excellent durability to maintain this high initial reflectance over the lifetime of a plant. The most common and mature type of solar reflector is the silvered-glass mirror. It consists of a front layer of special solar glass with high transmittance, which provides excellent front protection and a smooth base for the underlying reflective layer. Silver is one of the materials with the highest solar reflectance and is used as the reflective coating layer. The backside of the reflector is usually protected by a copper layer and a protective paint system with two to three different paint coatings. Even though this type of reflector is optimized for use in CST systems, it is prone to degradation [6]. The two main types of permanent degradation are the corrosion of the reflective silver layer [7] and changes in the glass cover. These changes are mainly surface defects due to mechanical attack (e.g., by airborne particles [8] or surface contact-cleaning [9]) or chemical reactions [10] (e.g., induced by UV radiation or humidity and moisture). Both of these degradation types potentially lead to a direct decrease of the reflectance of the reflector material. Other secondary types of degradation, mainly changes in the paint coatings, can indirectly influence the reflectance in the long term by leading to subsequent degradation of the reflective layer [11,12]. Reported degradation rates in the literature are rather low, at 0.1–0.2 % per year [7,13]. Higher degradation rates can be provoked by exposure at sites with high corrosivity or erosion potential or by the use of low-cost materials of unproven durability. A form of reversible degradation is the soiling of the reflectors. Dust and other particles can settle on the reflector surfaces and directly decrease the reflectance of the material. Ways to counteract soiling exist, for example by using anti-soiling coatings [14,15] and, mainly, by regular cleaning of the reflector surface [16,17]. Strongly varying soiling rates, from below 0.2 % up to over 2 %/day are reported in the literature [18,19], which, depending on the site, makes continuous cleaning mandatory to maintain high reflectance levels.

The reflectance, ρ, is a complex physical parameter, and its measurement depends on many secondary parameters that are used for its determination [20,21]. The main parameters are the incidence angle, Θ_i, and wavelength, λ, of the incoming irradiation, as well as the acceptance angle, φ, which is defined by the opening cone of the reflected light beam intercepted by the detector or the receiver, and which determines the amount of scattering away from the perfectly specular direction that is included in the measurement or captured by a receiver. A scheme with the representation of the important geometric parameters is displayed in Fig. 1. The most significant reflectance parameter for CST systems, which defines the amount of irradiation that can be focused onto a receiver, is labeled solar-weighted near-specular reflectance, $\rho_{s,\varphi}$, often called solar specular reflectance for the sake of simplicity [22,23]. The term solar refers to the weighting of the spectral reflectance over the whole solar range, usually defined as $\lambda = [320, 2500]$ nm, with a

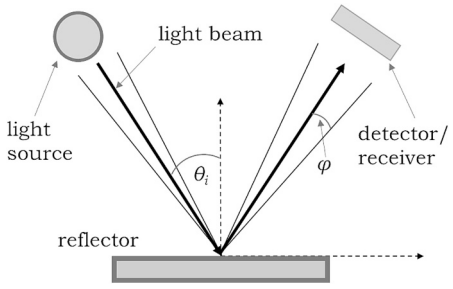

Fig. 1. Schematic presentation of reflection with important parameters. Incidence angle Θ_i and acceptance angle φ.

standard solar irradiance spectrum [24]. The term (near-)specular refers to the reflectance measured with a relatively small acceptance angle (usually below 150 mrad). Other parameters that lack certain information, are often measured due to technical limitations. These are mainly the spectral and solar-weighted hemispherical reflectance, $\rho_{\lambda,h}$, which neglects the scattering information, and the monochromatic specular reflectance, $\rho_{\lambda,\varphi}$, at single wavelengths or narrow wavelength bands, where the spectral information is limited.

The incidence and acceptance angles valid for CST systems are technology, site, time and location (in the solar field) dependent. Usually, mean values for specific sites are used to provide a significant value for a concrete case (CST plant). The two commercially most important technologies are parabolic-trough collector (PTC) systems, where one-axis tracked line-focusing collectors are used, and central receiver systems (CRS), in which large fields of two-axis tracked heliostats focus onto a receiver point on top of a central tower. In general, CRS systems exhibit smaller acceptance angles than PTC systems. The most widely cited value for the acceptance half-angle is $\varphi = 12.5$ mrad. It is perceived as the most suitable value for PTC standard designs [25,26] and it lies in the appropriate range for CRS systems [27], even though for the latter, smaller angles are often relevant. Several studies investigated the incidence angles occurring in both technologies calculated over a whole year in all parts of this type of plants. Mean values of around $\Theta_i = 30°$ were found for both technologies and various locations, with a range from near-normal to over $\Theta_i = 70°$ [28]. These results were confirmed in [27], where incidence angles for PTC and CRS were determined together with the effect they have on the reflectance depending on the reflector type. In addition, a method to predict the angular reflectance behavior is presented along with its experimental validation. These values may change when different designs and locations are investigated. For the present study, the solar near-specular reflectance at the selected incidence and acceptance angles for the specific plant is referred to as the

"reflectance of interest" (*ROI*), as the significant value for the specific case.

An overview of measurement techniques and instruments determining the reflectance in the CST sector is presented in [29]. Nowadays, the spectral specular reflectance in the relevant ranges can only be measured with advanced laboratory equipment. Few prototypes exist in specialized laboratories worldwide, without any commercial devices available [30,31]. The spectral near-normal hemispherical reflectance can be measured with standard spectrophotometers, which neglects the influence of the small-acceptance-angle scattering as well as off-normal incidence. These measurements are sufficient for highly specular reflectors, which is the case for new silvered-glass, for example. For degraded and especially soiled reflectors, as well as alternative reflector materials, the scattering effect cannot be neglected, and the specular measurement is necessary.

For practical reasons, operation and maintenance (O&M) of CST systems rely on the measurement of reflectance directly in the field, without the possibility of performing those measurements in the laboratory. A series of commercial portable reflectometers are available on the market for this purpose nowadays. Some of these devices were specifically designed for the use in CST systems, while others are adopted from other industries where similar measurement requirements apply. All available devices have certain limitations with respect to the measured reflectance parameters, resulting in potential differences from the *ROI*. For example, all devices measure at a fixed near-normal incidence angle ($\Theta_i < 20°$), with larger typical values for existing plants. Some of the devices measure at fixed acceptance angles, considerably higher than the realistic range for CST systems, to allow easier execution of the measurements. Few reflectometers allow the measurement at very small acceptance angles or allow the selection of a series of angles. The smaller the acceptance angle of a device, the higher is the need for precision in aligning the reflectometers relative to the surface to be measured. In [32] the main commercial reflectometer models are studied to evaluate the effect that different measurement parameters have on the results for various materials.

In-field soiling measurements are of special interest due to the high impact they have on reflectance, potentially decreasing the *ROI* and, with it, the optical efficiency of the whole solar field considerably. In addition, soiling develops much faster than the different mechanisms of permanent degradation. Consequently, regular measurements with relatively high frequency, up to daily, may be necessary, depending on the use case. Usually, the cleanliness, ξ, of the reflectors is determined by relating the reflectance at a point in time to the initial reflectance in the clean state. The cleanliness is used for different O&M tasks. Firstly, it can serve as an input parameter for yield calculations of the plant [33]. Secondly, depending on the strategy, cleaning tasks are scheduled when certain cleanliness thresholds are reached. This threshold depends on the balance between the cleaning effort (energy, labor, water usage) and the necessary minimum cleanliness for efficient operation [34,35]. Several studies investigated the optimal measurement procedures using portable reflectometers to minimize the number of measurements and obtain representative values for whole solar fields [36–38]. The cleanliness can be determined with the different reflectance parameters described above, the most significant one being the *ROI*. This is why the cleanliness determined with the portable reflectometers does not give the ideal results. Further techniques to assess soiling in the solar fields are being investigated without reaching the maturity of the reflectometer measurements, some of them adapted from the PV industry. One way to reduce the labor of the measurements is through the use of autonomous sensors [39–41]. These use different stationary setups to perform automatic measurements on material samples, but not the actual reflector facets. Measurements are based on reflectance or other parameters to be measured (e.g. the transmittance of glass specimens). Another technique is the image-based measurements [42–45], which mainly increase the covered area. Spatially resolved determination of the cleanliness, usually involving correlations to reflectance measurements, can be done manually or semi-automated by cameras mounted on trucks or drones [46]. A third option is the use of soiling forecast models [47,48]. They use physical or empirical models to predict the soiling, generally with input parameters such as airborne particle density, wind, and humidity.

One option to improve the results and add significance to the most common portable reflectometer measurements nowadays is using correlations between the readings obtained by reflectometers and the *ROI* [49]. Accordingly, the cleanliness determined based on the *ROI* is labeled cleanliness of interest (*COI*). Such correlations are expected to be strictly specific to the adopted reflectometer applied to the given solar plant. Correlations of this kind were established in different studies, for example in [39,50–52] for different reflectometer combinations, with linear relations between the results from the different devices. These studies focus on the comparison of the different reflectometer models but lack a direct relation to the more significant *ROI* and are limited to relatively low-soiling cases. As an alternative to these correlations, in [53] a model is introduced to simulate the soiling behavior for different soiling types. The model parameters can be adapted with a limited set of measurements of spectral hemispherical reflectance and specular reflectance at a few wavelengths. With the adapted model, it is then possible to calculate the spectral specular reflectance as a function of the incidence and acceptance angles, and with that determine the above-mentioned correlations for different use cases. In that publication, indications are found that there is a strong dependence of the shape of the spectral loss induced by soiling on the soiling type (e.g. from different exposure sites), a fact that leads to case-specific correlations. This model was then used to establish example correlations between reflectometers and *ROI* in the appendix of [49]. Research published in the past has led to important progress in the knowledge about the correlations between the different reflectance parameters, but presented certain main limitations: limited number of reflectometers, lack of *ROI* and realistic outdoor data, as well as a limited soiling/cleanliness range.

Below, a study is presented in which correlations are developed between the measurements of all main reflectometer models used in the commercial CST plants and the solar specular reflectance. As a case study, the CIEMAT-Plataforma Solar de Almería (PSA), Spain, site is used and reflector samples with natural soiling, covering a wide range of cleanliness levels, are included. The results allow the standard reflectometer readings to be translated directly to the most significant target value and thereby adding value to the measurements without additional effort.

2. Methodology

In this section, the methodology to derive the correlations between portable and laboratory devices in soiled reflectors is presented. First, the reflector material used and the outdoor exposure campaign to achieve realistic soiling in such material are explained. Secondly, the measurement equipment employed and the procedures for determining the different reflectance and cleanliness parameters are detailed.

2.1. Reflector samples and exposure campaign

The material used for the entire measurement campaign is a commercial silvered-glass mirror of 4 mm thickness manufactured by Rioglass. The company has a long track record in the supply of solar reflectors for CST projects [54,55]. Samples were cut from full size heliostat facets in pristine condition before any prior exposure, to a size of approximately 10 x 10 cm^2. High specular reflectance and homogeneity of the material were verified by reflectance measurements before the campaigns started, to avoid negative influence on the soiling measurements.

The exposure site, the PSA, is a large-scale research facility focused on CST technologies in southern Spain. It is located in the semi-arid region of Tabernas. A detailed characterization of the environmental

parameters at the PSA was published in [56]. The main characteristics reported are mean annual values for temperature (18.3 °C), relative humidity (59.5 %), and wind velocity (3.2 m/s). A local soiling analysis showed that its main constituent is quartz, with lower quantities of clay and carbonate minerals. An exposure campaign was designed to provide reflector material covering a wide range of soiling levels, without relying on different exposure durations. For that, the positioning of the samples at different inclination angles to the horizontal was chosen, resulting in inclination-dependent soiling [57]. Samples were exposed on a specially designed rack with holders of seven different inclination angles, from 0° (horizontally facing upwards) to 180° (horizontally facing downwards), in evenly distributed inclination angle steps, as displayed in Fig. 2. The rack is oriented so that the tilted samples face west, which is one of the main wind directions at the PSA. Three samples were exposed per inclination, totaling a number of 21 samples (labeled S1 to S21) in the main campaign. Six additional samples (S31 to S36) were exposed during an extra campaign at the two first upward facing inclination angles. The extra campaign was conducted after detecting a large gap in the desired soiling levels of the samples from the main campaign. The first main campaign comprised an exposure duration of two weeks during the summer of 2023 and the extra campaign lasted ten days in the spring of 2024.

2.2. Measurement devices

The main and most commonly used commercial reflectometers in CST plants were included in the experiments. The reference parameter, the *ROI*, was determined using the S2R laboratory reflectometer. Five of the handheld reflectometers (D&S-15R, D&S-RGB, Condor, pFlex and SOC410) were specifically designed for specular reflectance measurements in CST systems. The other two portable devices (CM700d and ZGM1130) were adopted from other applications (e.g. paint coatings, polymers and related materials), in which color and gloss measurements are the primary concern, respectively. All devices provide values for monochromatic specular reflectance. Most devices determine the specular reflectance directly, except for the SOC410 and CM700d, which determine the specular value by subtracting the diffuse reflectance from the hemispherical one. Additional details on the measurement and handling parameters can be found in [29] and the respective user manuals. All portable devices are displayed in Fig. 3.

2.2.1. Portable reflectometers

The D&S-15R reflectometer, from Devices & Services, developed in the 1980 s at Sandia National Laboratories [58], is the device with the longest track record in the CST industry. It measures at near-normal incidence of $\theta_i = 15°$, at a wavelength of $\lambda = 660$ nm. Acceptance angles of $\varphi = \{3.5, 7.5, 12.5, 23.0\}$ mrad are available for measurements. In the presented campaign, $\varphi = 12.5$ mrad was chosen as a representative value for CRS and PTC technologies. The updated D&S-15R-RGB model (hereinafter labeled as D&S-RGB) offers the capability to measure at several wavelengths, $\lambda = \{460, 550, 650, 720\}$ nm, with an additional white light source for improved spectral evaluation [29], and an additional acceptance angle of $\varphi = 2.3$ mrad. The available φ of the D&S models are considerably lower than those of the other devices. This has the advantage of representing more realistic and relevant values for CST cases, but comes with the disadvantage of more complex handling. The small acceptance angle makes the manual alignment of the device relative to the reflector surface necessary, which is achieved by the adjustment of three screws on the base of the device, to assure the correct positioning of the reflected light beam. This is especially important in the case of curved reflectors and material with varying thickness of the front glass cover.

The Condor reflectometer by Zepren [59], developed as a collaboration between the University of Zaragoza and Abengoa, measures at $\theta_i = 12°$, at six discrete wavelengths, $\lambda = \{435, 525, 650, 780, 940, 1050\}$ nm, and an acceptance angle $\varphi = 145.0$ mrad. Due to the higher acceptance angle, alignment of the device is not necessary, which facilitates the measurement process in the solar fields. Each λ measurement is achieved by its own light source and detector combination.

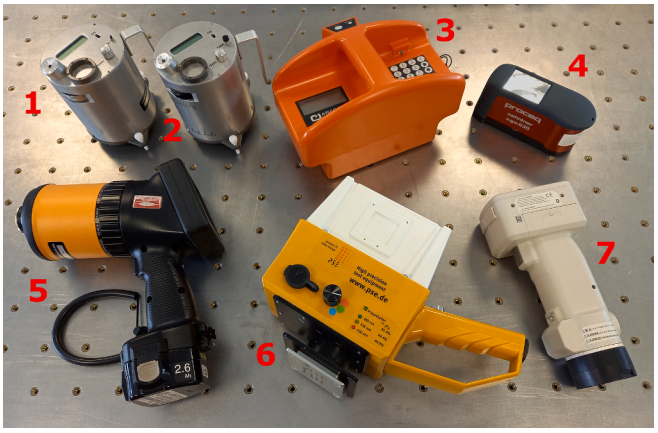

Fig. 3. Reflectometers used in this study: 1) D&S-15R, 2) D&S-RGB, 3) Condor, 4) ZGM1130, 5) SOC410, 6) pFlex, 7) CM700d.

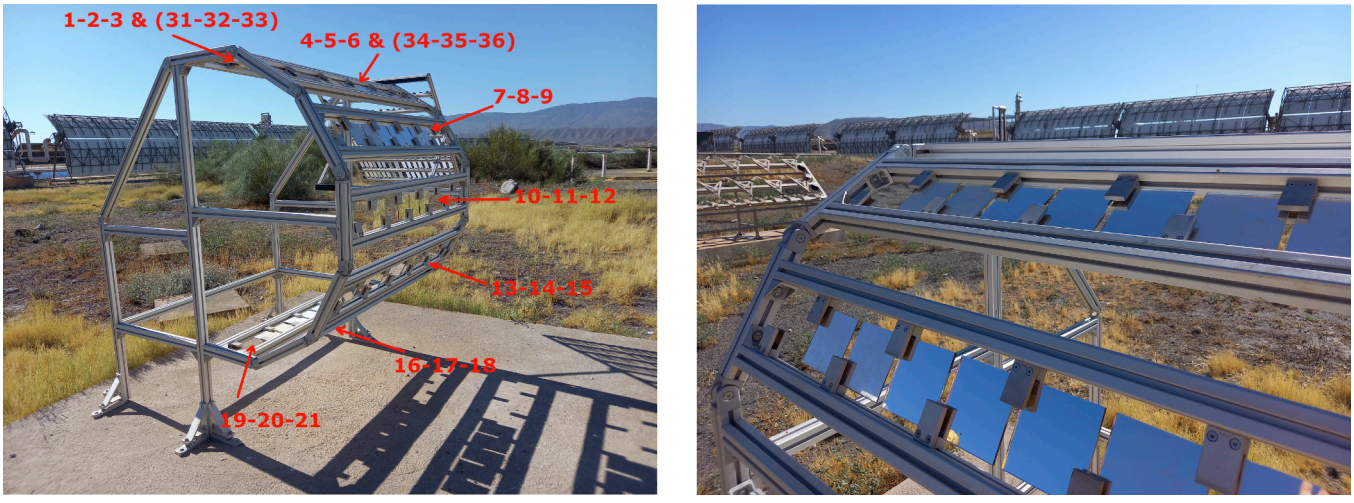

Fig. 2. Sample exposure rack with marked positions and sample numbers during main and extra campaign (left), detailed view of first inclination rows from the horizontal, with sample holders (right).

These are positioned in a straight line and separated from each other by approximately 1.5 cm. This way, execution of measurement implies measurements on six slightly different points on the reflector surface, with a total distance of ca. 10 cm. The Condor internally calculates the solar-weighted reflectance based on the six wavelength measurements, which implies an additional advantage of this device.

The pFlex by PSE, developed in collaboration with Fraunhofer ISE, measures at $\theta_i = 8°$ at three different wavelengths, $\lambda = \{470, 530, 630\}$ nm with an intermediate acceptance angle (compared to the other devices) of $\varphi = 67.2$ mrad. As for the Condor, no manual alignment is necessary during the execution of the soiling measurements. The λ to be measured is selected and the measurements are executed manually. Handling and data storage are performed with a Bluetooth connected smartphone.

Surface Optics developed the SOC 410-Solar (short: SOC410) in collaboration with the U.S. Naval Air Systems Command. The SOC410 measures at $\theta_i = 20°$ in the whole solar spectrum via seven λ ranges of varying bandwidths with an acceptance angle of $\varphi = 67.2$ mrad, slightly higher than the pFlex. The wavelength ranges have a similar width as the other devices for the lower wavelengths, but especially at higher wavelengths these cover a broad range of 700–800 nm. An integrating sphere is used to measure hemispherical and diffuse reflectance, from which the near-specular reflectance is determined. As for the Condor, the solar-weighted reflectance is determined internally by the device. The SOC410 is relatively sensitive to the thickness of second surface reflectors, and, according to the manufacturer, it should be aligned by the company for the corresponding thickness. The device available for this campaign was aligned for first surface reflectors. To account for that, an adapter was manufactured that slightly tilts the reflectometer relative to the surface thereby ensuring the correct positioning of the reflected beam inside the integrating sphere. Consistency of the measurements was confirmed before the execution of the campaign, however, it must be noted that this is not the manufacturer's recommended procedure, and an influence on the results cannot be excluded.

The CM700d by Konica Minolta is a device developed to determine the color of surfaces. It is widely used for highly standardized measurements in sectors such as the automotive industry and other paint-related applications [60]. Its use for quality control by mirror manufacturers and in CST plants has been reported in the past. The device measures in a spectral range of $\lambda = [400, 700]$ nm with 10 nm steps. The incidence angle is $\theta_i = 8°$. The exact acceptance angle is not given by the manufacturer, but the effective φ has shown to be similar to the one from the pFlex device [32]. The CM700d, as the SOC410, uses an integrating sphere for the hemispherical and diffuse reflection measurement, and the near-specular reflectance is then calculated by the subtracting the two magnitudes.

The ZGM1130 by Zehntner is a commercial glossmeter. Although glossmeters were not recommended in several publications in the past [22,26,29], they are commonly used in-field to determine reflectance in several commercial plants and were thus included in this study. Gloss measurements are widely used in industries such as paint and coating manufacturing [61] and are highly standardized, for example under ISO 2813 [62]. A variety of commercial equipment exists on the market and the ZGM1130 was selected for this campaign due to information that this model is used in plants, by personal correspondence. Due to the standardization of measurements, only small differences are expected between different models. Following the standards, the ZGM1130 measures at $\theta_i = 20°$, having a white LED source with a peak at $\lambda = 460$ nm. A rectangular opening determines the acceptance angles for this device, in contrast to the round openings of the other devices. This results in two acceptance angles determining the included scattered light, $\varphi = 15.7$ mrad parallel to the plane of reflection and $\varphi = 31.4$ mrad perpendicular to the plane of reflection. To give a single value for the acceptance angle of this device, the mean of the two angles can be taken, $\varphi = 23.6$ mrad, assuming isotropic scattering behavior. Table 1 presents a summary of all the main parameters of the seven reflectometers included in this study.

Table 1
Used reflectometer models with main measurement parameters, according to manufacturer information.

Model	θ_i [°]	φ [mrad]	λ [nm]	measurement spot diameter [mm]
D&S-15R	15	3.5, 7.5, 12.5, 23.0	660	10.0
D&S-RGB	15	2.3, 3.5, 7.5, 12.5, 23.0	460, 550, 650, 720	10.0
Condor	12	145.0	435, 525, 650, 780, 940, 1050	2.7
pFlex	8	67.2	470, 530, 630	10.0
SOC410	20	52.4	335–380, 400–540, 480–600, 590–720, 700–1100, 1000–1700, 1700–2500	6.4
CM700d	8	*	400–700 (10 nm steps)	8.0
ZGM1130	20	23.6**	white LED, with peak at 460 nm (smaller at 570)	9.8

*Acceptance angle not given by the manufacturer.
**Mean value of the two acceptance angles, perpendicular and parallel to plane of reflection.

2.2.2. Laboratory reflectometer S2R

The Spectral Specular Reflectometer (S2R) is a laboratory reflectometer, designed as an accessory for the commercial Lambda 1050 spectrophotometer by Perkin Elmer, based on the General Purpose Optical Bench (PELA1003) [54]. The device has the capability to determine the spectral near-specular reflectance, $\rho_{\lambda,\varphi}$, in the solar range, $\lambda = [320, 2500]$ nm wavelength, with θ_i ranging from near normal (ca. 10°) to close to 90° and $\varphi = [7.4, 107.4]$ mrad. With $\rho_{\lambda,\varphi}$, the solar-weighted reflectance can be determined by the weighting with the solar irradiance standard spectrum IEC 60904 [24]. For this campaign, measurements were performed at $\theta_i = \{15, 30, 60\}°$ and $\varphi = 12.5$ mrad. As explained in the introduction, with these incidence angles the important range appearing in commercial plants is covered by this equipment. The φ selected in this case represents a realistic and the most commonly used value. In Fig. 4 left, the measurement setup with the sample in the center is displayed. In Fig. 4 right, the position of the illuminated measurement spot can be identified. Fig. 5 presents the simplified light path of the measurement setup together with its main components.

2.3. Measurement procedure

To determine the correlations between the measurements with the different devices, it was chosen to compare results obtained on the exact same measurement spots. As natural soiling always possesses a certain degree of spatial heterogeneity, reflectance values on soiled surfaces can vary substantially across the surface area [43,63]. Taking values of the same measurement spots minimizes this effect, with the limit of the precision of the measurement point selection and differences in measurement spot sizes.

The used laboratory equipment S2R allows for a very precise positioning of the sample to be measured without contact between equipment and the reflector surface (Fig. 4 right). The portable devices, by contrast, must be placed manually on the sample, introducing positioning uncertainty and unavoidable surface contact. The contact between reflectometers and sample surface potentially alters the soiling on the surfaces. This is not problematic during outdoor measurements in commercial plants, as the affected area is minimal. However, for the here presented study, this effect has to be avoided, as this could compromise the comparability of consecutive measurements with different devices.

To address both issues of the positioning and to avoid contact, custom measurement masks were specifically designed for the different

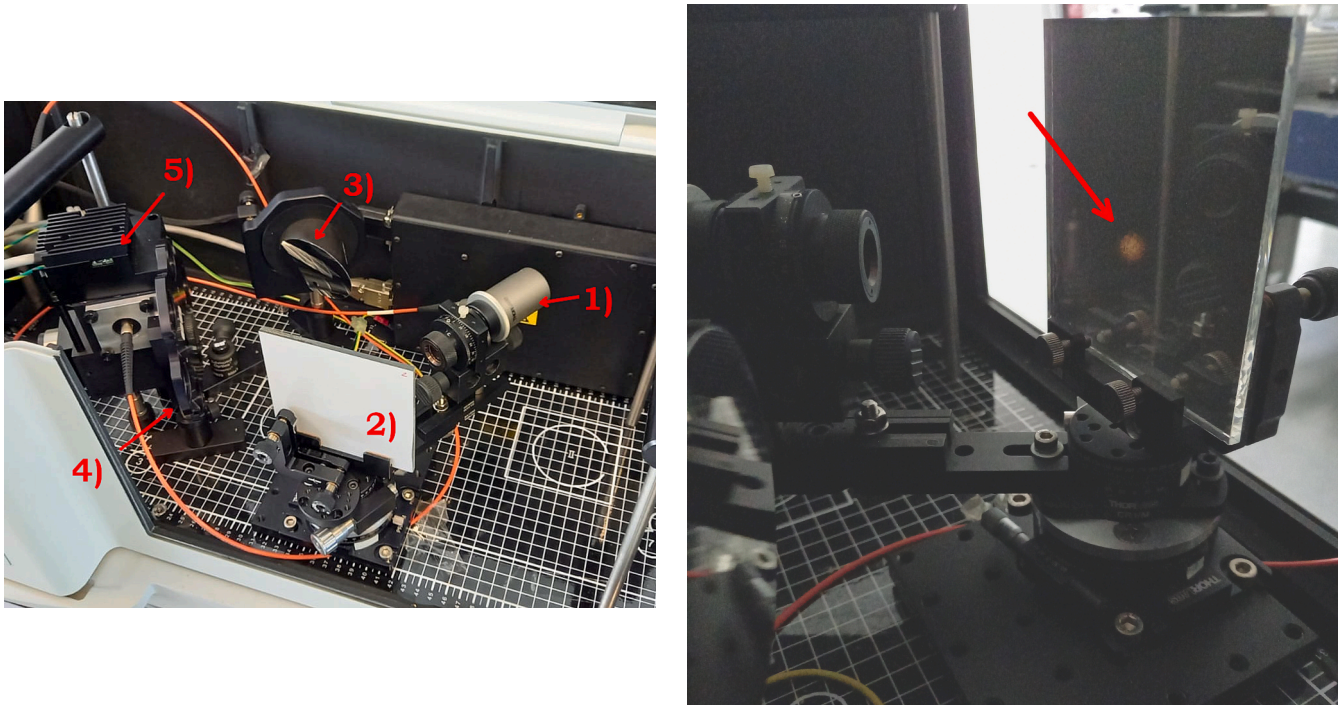

Fig. 4. S2R measurement compartment with soiled reflector placed in sample holder (left: 1. light source, 2. mirror sample, 3. off-axis parabolic mirror, 4) aperture wheel acceptance angle selection, 5. integrating sphere with detector). Position of the visible measurement spot on sample marked with red arrow (right).

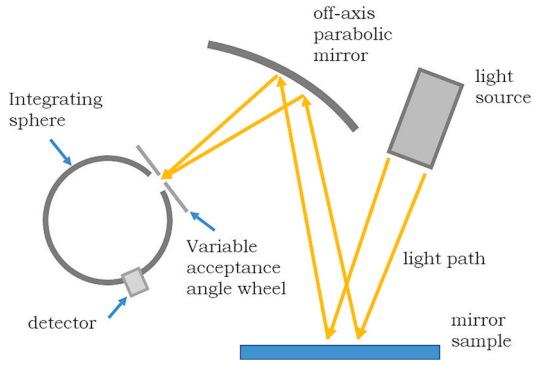

Fig. 5. Diagram of the main light path and components of the S2R setup.

reflectometers. The masks have the tasks to slightly elevate the devices, by approximately 1 mm, and allow for a more precise positioning of the measurement spot. Preliminary measurements confirmed that elevating the reflectometers had a negligible effect on the results. In Fig. 6, the designed masks are displayed, together with the adapter developed for the SOC410. No masks were used for the SOC410 and the ZGM1130 as they had shown a higher sensitivity to the slight lifting of the equipment from the reflector surface. For these two devices manual placement was used, adding uncertainty to the positioning for measurements.

Due to the more precise positioning of the samples in the S2R compared to the reflectometers, for the S2R, one measurement was performed per sample. In preliminary measurements, it was confirmed that the variations between repeated measurements on the same spot were below 0.001. By contrast, for the reflectometers the measurement was repeated three times, to account for slight changes in the positioning. The average of the three measurements was then taken as the value for the respective sample.

As the Condor uses different measurement spots for the different wavelengths, the mask for the Condor allows the movement of the device and the positioning for the respective wavelength on the samples.

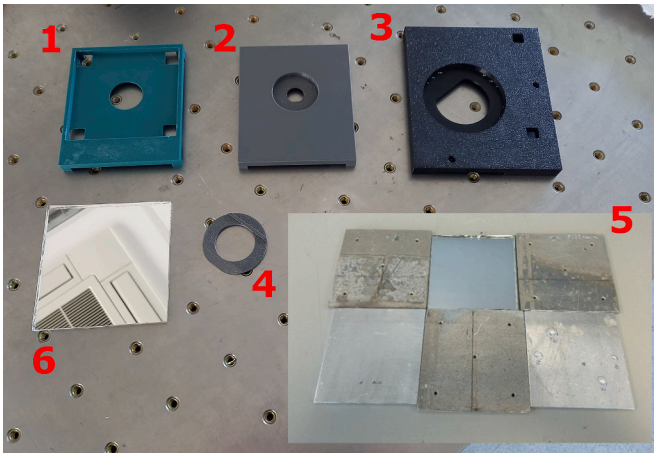

Fig. 6. Measurement masks designed for the different reflectometers: 1) pFlex, 2) CM700d, 3) D&S-15R, 4) adapter for SOC410, 5) Condor, 6) 10x10 cm^2 sample for reference.

During the evaluation of large reflector facets, the Condor is able to calculate the solar-weighted reflectance based on the six single wavelength values. Due to the repositioning between measurements, this calculation could not be utilized for these experiments.

All samples from the outdoor campaign were measured, first with the S2R and followed by the portable reflectometers. Measurements of a clean sample of the same material were performed as well. The cleanliness, ξ, was determined for all devices and samples by dividing the soiled value by the clean one:

$$\xi = \frac{\rho_{soiled}}{\rho_{clean}} \quad (1)$$

Correlations are then derived by directly comparing measurements per sample between the S2R and the respective reflectometer. The reflectance or the cleanliness can be used to derive correlations depending on

the interest of the user. As all these direct comparisons show a highly linear behavior, linear trend lines (equation $y_{target} = a^{*}x_{base} + b$ with the slope a and the y-intercept b) are calculated for the different cases by least-square fitting, together with the corresponding coefficients of determination R^2, as measures of the quality of the linear fit. The closer the R^2 is to one, the better the linear fit represents the data.

3. Results

In this section, the results are presented, beginning with a qualitative visual evaluation of the soiling pattern forming on the exposed samples. Then, the results from the S2R measurements are analyzed, including the spectral and solar-weighted reflectance of the different soiling levels. This is followed by the spectral comparison of all devices to the respective S2R values. The main results are then shown, presenting the correlations to the previously defined target values *ROI* and *COI*, and finishing with a comparison of such correlations to data from several studies published by different groups in the past.

3.1. Qualitative visual inspection of soiled samples

In Fig. 7, images of samples of all soiling groups (one group is defined by the same tilt and the same exposure period, e.g., samples 1–3) are presented. It can be seen that a relatively homogeneous soiling develops over the surfaces, but notable local heterogeneities can be distinguished, which seem to be more pronounced in the case of the second campaign (sample 31 and 33). This could be caused by some nighttime dew formation on the samples and the local accumulation of particles. In addition, the spots where the sample holders were fixed, and thus protected from soiling on the sample edges are visible. Subjectively, the strongest soiling can be seen on the first samples, horizontally facing upwards, and a decreasing level of soiling at higher inclination angles, closer to vertical and facing downwards. The level of soiling during the extra campaign is considerably lower than for the first one, with the two samples S4 and S31 shown in the image coming from the same inclination.

3.2. Laboratory measurements – spectral specular reflectance

In Fig. 8, the spectral near-specular reflectance measured with the S2R is displayed for all samples, used as the target value for the comparison to the reflectometers, at $\theta_i = 30°$. Towards the higher end of the spectrum, close to 2500 nm, the noise level of the measurements is high. This does not negatively affect the significance of the measurement as it is limited to a small part of the spectral range, where the solar irradiation portion is low. Some samples from the first campaign were not measured, namely samples 15 to 21, as preliminary measurements had shown, that from samples 10 to 21, cleanliness values are close to 1 and thus data does not contribute new information. Several groups of reflectance values can be distinguished. Samples that were placed horizontally (1 to 3) and near horizontally (4 to 6), show the lowest reflectance in the range of 70 % over most part of the spectrum, with the mean of the horizontal ones slightly higher than that of the tilted ones. The samples 7 to 9, the next further tilted group shows higher reflectance values, still below 80 %, with little difference between the samples. From sample 10 on, vertical and down-facing, the reflectance is already in the range above 90 % in the main part of the spectrum and with that close to the value in the clean state, which is represented by S40 (yellow line). Samples 31 to 36 were positioned during the extra campaign in the same way as samples 1 to 6 during the main campaign. As can be seen, they successfully fill the gap in the 80 % range (dashed lines), as intended for this extra exposure campaign. For all soiling levels, the reduction in reflectance is relatively constant over the whole spectral range.

To better visualize the spectral behavior of the soiling, and the reduction in reflectance it causes, in Fig. 9, the absolute reflectance difference to the clean material is displayed. It can be seen that the reflectance reduction is fairly constant over a large part of the spectrum. Stronger spectral variations can only be seen for wavelengths below 400 nm and above around 2200 nm. The strongest reflectance reduction is in the visible range, with a slight decrease towards higher wavelengths. The variations over the spectrum are more pronounced the higher the total soiling level is. As the portable reflectometers mainly measure in the above-mentioned range, a limited spectral influence on the reflectance decay by soiling is expected when using such equipment. Only three of the SOC410 wavelength bands lie considerably below 400 nm or above 1050 nm, while the rest of all the reflectometer values stay well within these limits.

As mentioned, the reflectance at $\theta_i = 30°$ is shown in Fig. 8 and Fig. 9, because it is the main value later used for the correlations. The general behavior is the same for the other measured θ_i, with decreasing total values at higher incidence angles. In Fig. 10, the solar-weighted values are displayed for the three measured θ_i and all samples. For the most heavily soiled samples, the differences between 15° and 60° lie in the range of 6 to 10 %pt, while for the cleaner ones they are in the range of 1 to 2 %pt and an average of all differences of 4.4 %pt. Differences between 15° and 30° measurements are rather low, with a maximum difference of 1.7 %pt for the most soiled sample and an average of 0.4 %pt. At low soiling levels ($\xi > 0.9$), differences are lower than 0.2 %pt.

3.3. Comparison of the spectral behavior of all devices

To compare the spectral behavior of the different devices, the data for two exemplary samples, a clean sample and one of the most soiled ones, are presented for all devices. In addition, the spectra measured with S2R at the three different incidence angles are included, to show

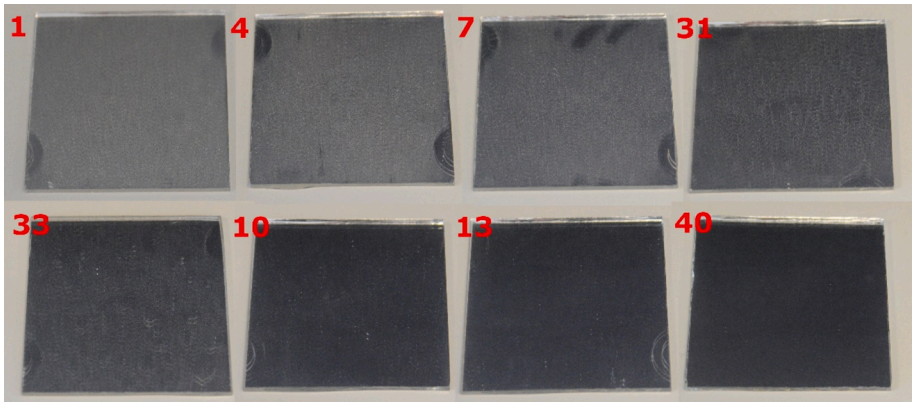

Fig. 7. Images of soiled samples, from every group, from lowest cleanliness to highest (samples 1, 4, 7, 31, 33, 10, 13, 40), 40 is clean sample for reference.

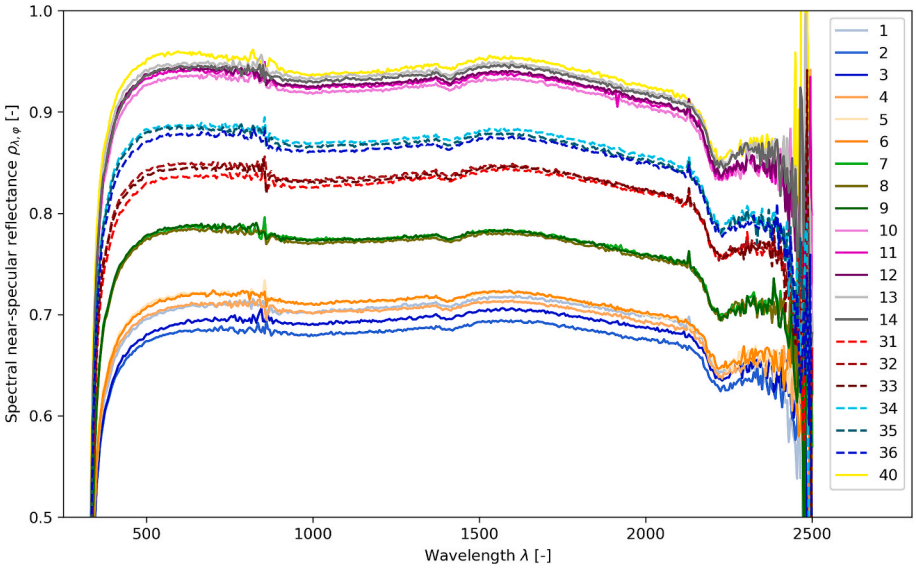

Fig. 8. Reflectance spectra measured with S2R at $\theta_i = 30°$ and $\varphi = 12.5$ mrad for all 20 soiled samples measured, 31–36 from extra campaign with dashed lines, 40 is clean sample.

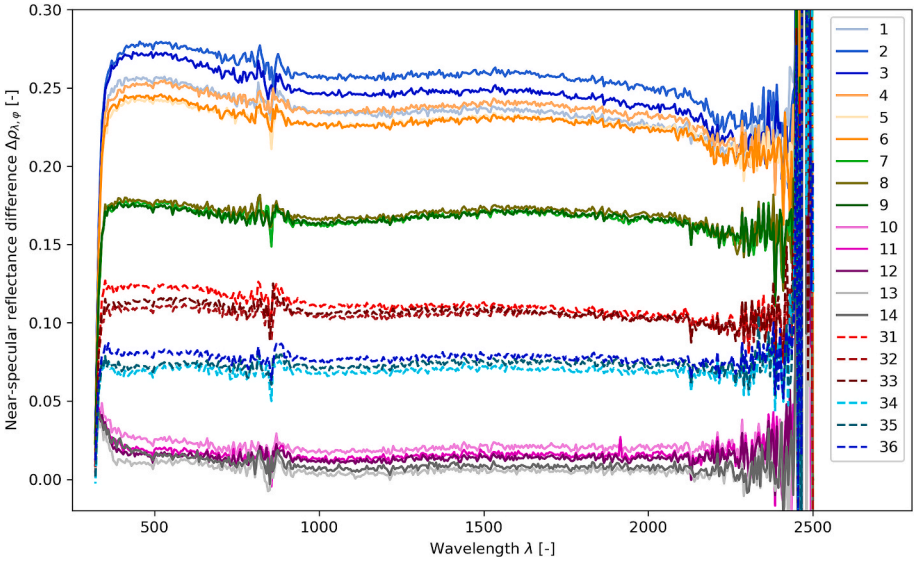

Fig. 9. Difference in reflectance measured with S2R at $\theta_i = 30°$ and $\varphi = 12.5$ mrad for all measured samples between clean and soiled, 31–36 from extra campaign with dashed lines.

the influence of this parameter and its variation with soiling level. The *ROI* considered in the present study, the solar specular reflectance at 30° of incidence and 12.3 mrad of acceptance, is displayed as a horizontal grey line. In Fig. 11, the clean sample data and in Fig. 12 the soiled sample data is shown. As expected, the general behavior is a higher reflectance for the clean sample for all devices, as well as smaller differences between devices for that sample. As explained in the previous chapter, for the clean sample (see Fig. 11), the S2R values with different incidence angles vary only slightly. Also, the differences of the portable reflectometers from the S2R are low, with a mean difference of all spectral values of 0.004, which can be explained by the low scattering on this sample and with that the negligible influence of the variation in acceptance angle between devices. The highest differences are detected for the CM700d (mean difference of 0.012), which was reported in the past due to calibration issues [32]. The value of the SOC410 at the highest wavelength also shows a considerable difference to the S2R values (0.037). This can be explained by the covered wavelength band of the SOC410 in this part of the spectrum, ranging from 1700 to 2500 nm, and this way representing the mean value of this whole part, where the S2R results show a considerable reflectance drop.

For the soiled sample (see Fig. 12), the overall reflectance is lower and differences between devices and incidence angles are higher. A small variation between 15° and 30° incidence angle of the S2R (mean spectral difference 0.007) is detected, compared to a considerably higher difference between 30° and 60° (mean of 0.055). Due to the nearly identical acceptance angle used with the D&S-15R and D&S-RGB, their values agree very well with the S2R value at 15° incidence. The highest differences from the S2R are detected for the Condor, in agreement with its highest acceptance angle. The values of pFlex, SOC410 and CM700d lie in between these, with the SOC410 being the lowest of these three, in accordance with its slightly lower acceptance angle. It is fundamental to acknowledge that these differences do not arise from measurement errors, but are due to the differently chosen acceptance angles.

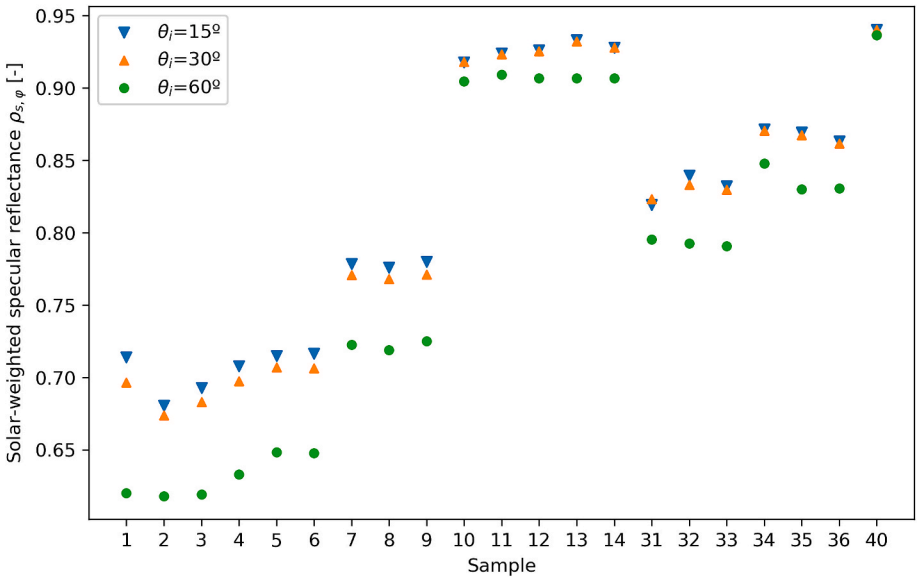

Fig. 10. Solar-weighted reflectance determined with S2R for all samples at three incidence angles (θ_i={15, 30, 60}°).

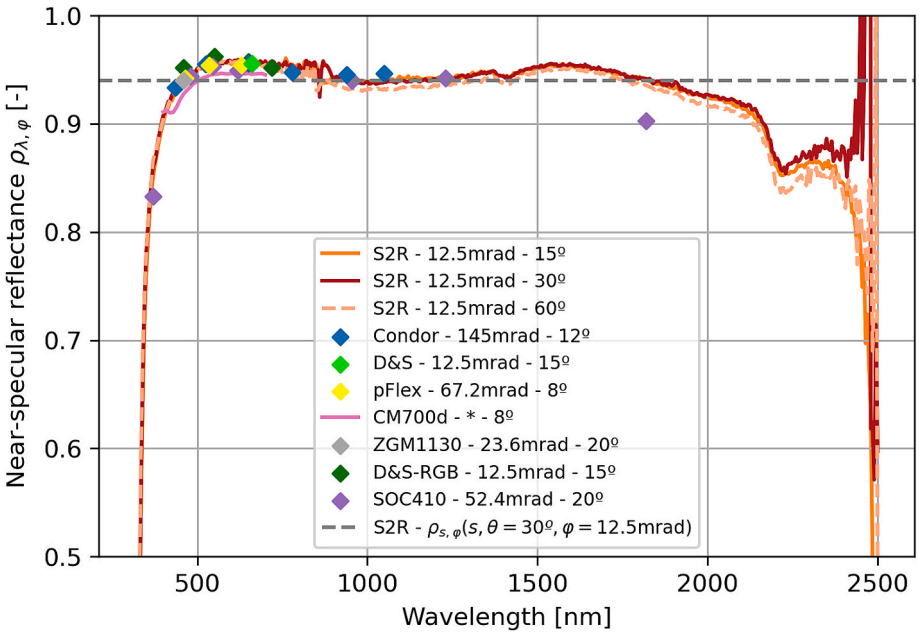

Fig. 11. Spectral specular reflectance of all devices and ROI for the clean reference sample. The values in [mrad] refer to the acceptance angle, and the values in [°] to the incidence angle.

Even though the ZGM1130 has a white LED source, emitting in the range of around 450 to 700 nm, its data is also included for both samples. The ZGM1130's strongest peak wavelength at ca. 460 nm is selected to represent its reflectance data in the spectral charts. Agreement with S2R measurements is very good for the clean sample and a slight overestimation of the reflectance can be detected for the soiled samples due to the higher acceptance angle of the device.

3.4. Standard deviations of portable reflectometer measurements

As the soiling on the sample surfaces shows a certain degree of heterogeneity, the standard deviation of the three measurements per sample with the portable devices gives an indication of the magnitude of the heterogeneity. In general, the standard deviations for all devices are rather low throughout the whole campaign. This was achieved by using the same measurement spots for all measurements, especially in comparison with past campaigns including measurements on larger areas, where the selection of the same spots was not used (see, for example, [50,52]). In Table 2, the mean values of the standard deviation over all specimens are presented per device. The total average of all devices is 0.0018, which is a low value. All the devices that used the measurement masks, the D&S models, Condor, CM700d and pFlex, show standard deviations well below 0.0015. The SOC410 and the ZGM1130, on the other hand, present higher values with means of 0.005 and 0.003, respectively, due to lower positioning accuracy. In Fig. 13, two graphs are shown that present the standard deviations of reflectance for all samples versus the mean reflectance values. On the left, the devices with all standard deviation values staying below 0.002 are displayed, without a clear tendency toward lower mean reflectance values. On the right, the rest of the devices are presented, with a tendency of higher standard

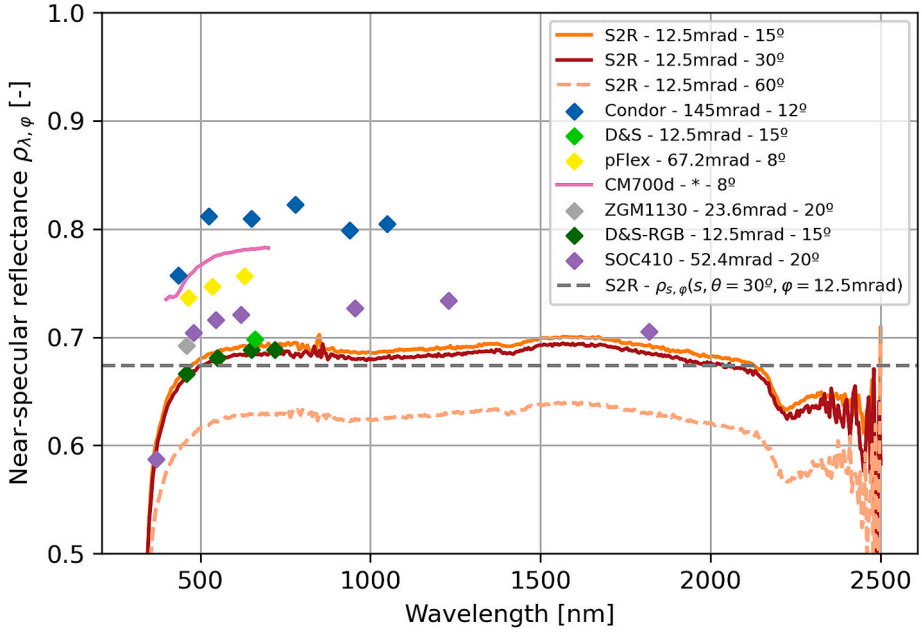

Fig. 12. Spectral specular reflectance of all devices and ROI for one of the most heavily soiled samples S2. The values in [mrad] refer to the acceptance angle, and the values in [°] to the incidence angle.

Table 2
Average values of standard deviations for all samples per devices, total average over all devices.

Device	D&S-15R	D&S-RGB	Condor	CM700d	pFlex	ZGM1130	SOC410	Total average
λ [nm]	660	650	650	650	639	white	620	–
Average standard deviation	0.0004	0.0005	0.0014	0.0005	0.0014	0.0032	0.0053	0.0018

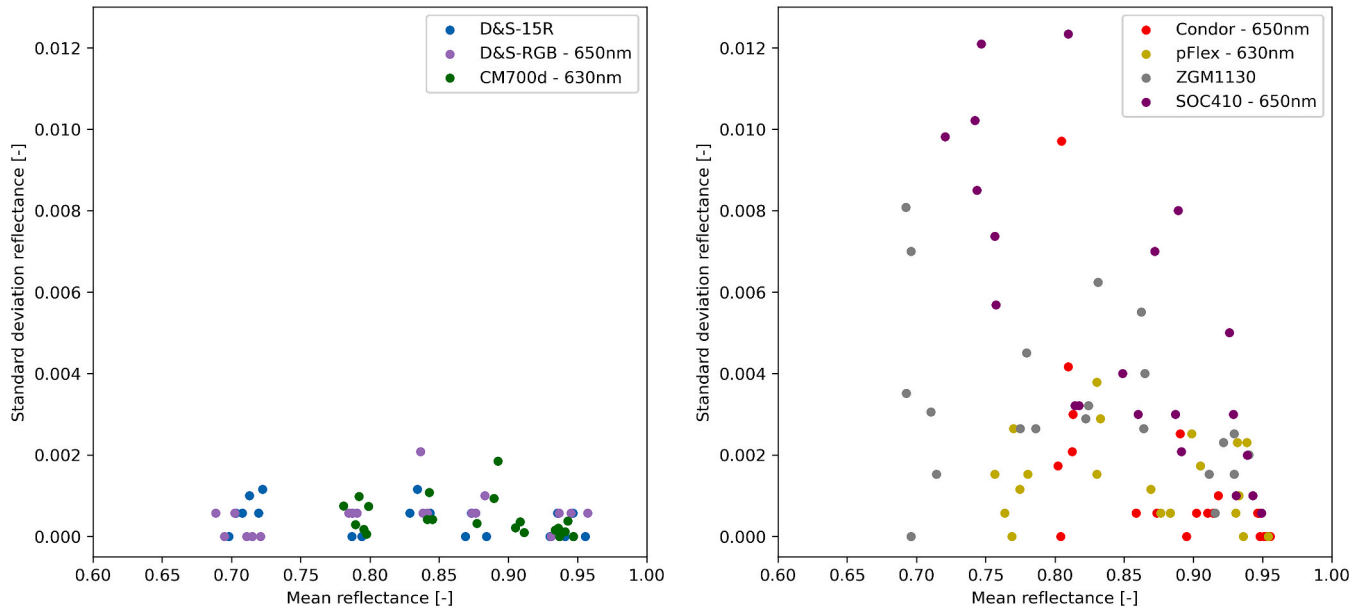

Fig. 13. Standard deviations of the reflectance measurement with the different reflectometers plotted versus the mean value.

deviations towards lower mean reflectance values (stronger soiling). Again, the higher values for SOC410 and ZGM1130 can be distinguished, with absolute maximum values of 0.012 and 0.008, respectively. Condor and pFlex deviations are lower, with a maximum outlier for the Condor of 0.01. The magnitude of all standard deviations does not have a considerable negative impact on the later developed linear correlations for any device, as is shown in the next section.

3.5. Correlations between reflectometer readings and values of interest

As explained in the introduction, the values of interest, to which the reflectometer readings should be translated, are *ROI* and *COI* computed with the spectra measured with the S2R at $\varphi = 12.5$ mrad and $\theta_i = 30º$, the most relevant values for the PSA case. These parameters may differ depending on the specific case of interest. To determine the correlation

between each portable reflectometer reading and this target parameter, the values are directly compared for all the samples included in this study with the different soiling levels. This is done directly for the reflectance and also with the cleanliness values.

To be able to compare the behavior of all portable devices, in Fig. 11, their values at a similar wavelength are plotted against the *ROI* (on the left) and *COI* (on the right). As all devices except for the ZGM1130 provide a value at a wavelength corresponding to red light, in the range of $\lambda = [620, 660]$ nm, these values are used in Fig. 11. For the ZGM1130, the white light value is taken as the only parameter produced by this equipment. The linear trend lines for all devices are included together with the corresponding equations and R^2 values. The line representing equality between devices (reflectometer value = *ROI* or *COI*, x = y) is displayed in grey.

Evaluating the reflectance data, the first main finding is that data from all reflectometers show a very linear behavior with negligible dispersion. This means all devices allow the determination of *ROI* and *COI* using the correlations. R^2 values are all close to one, with most values being above 0.99, proving an excellent approximation of the linear equation. The Condor data shows a slightly lower value of $R^2 = 0.987$, which might be explained by the small measurement spot size, compared to the other devices. As the other devices measure on a larger area, the spatial heterogeneity of the soiling can lead to higher variations in the results. During normal in-field measurements with the Condor, measurements on six spots are combined, leading to a similar covered area compared to the other devices.

The second main finding is that the three devices with the lowest acceptance angle, and with that the closest to the target parameter, lie very close to the *ROI* and *COI*. Both D&S devices have the same acceptance angle as the target parameter and thus the slope of the linear equations are close to one ($a_{D\&S\text{-}15R} = 1.02$, $a_{D\&S\text{-}RGB} = 0.99$). The acceptance angle of the ZGM1130 is higher and thus the differences to the target value are greater at stronger soiling levels, due to stronger scattering, resulting in a slightly higher slope ($a_{ZGM1130} = 1.05$).

All the other reflectometers have considerably higher acceptance angles, which leads to larger differences at higher soiling levels. This results in higher slopes of their linear trend lines, mainly depending on the acceptance angle. The SOC410 and Condor have the lowest and highest acceptance angle of this group, respectively, which results in the lowest and highest slopes. The differences due to the acceptance angle have no negative influence of the outcome of the target value when the correlations are used.

The general behavior is the same when evaluating the cleanliness instead of the reflectance (see Fig. 14 on the right). Due to normalization to the reflectance in the clean state, all trend lines coincide at 1. This mainly cancels the influence of the calibration of the devices, as well as the initial reflectance in the clean state, when comparing different materials.

In the following section, the same type of graph as shown above is displayed for all available wavelengths per device. D&S-15R and ZGM1130 are not included in this additional analysis as they only provide one spectral value, which is already included in Fig. 14.

Fig. 15 shows all D&S-RGB values versus the target value. As before, a favorable linear approximation is achieved for the evaluated parameters ($R^2 > 0.997$). The value at $\lambda = 460$ nm is slightly lower for the D&S-RGB (to the right of the x = y-line), which can be explained by the fact that this value already is in the spectral range where the reflectance shows a downward trend (compare Fig. 9).

In Fig. 16, the values for all wavelengths of the Condor are presented. As explained in the methodology, the devices apart from the D&S use higher acceptance angles to increase ease of use and reduce the need for alignment and user errors. The Condor design includes the highest acceptance angle of the included devices, which leads to the highest flexibility concerning thickness and curvature of the reflectors to be measured. On the other hand, due to the high angle, it shows the highest differences of all devices to the *ROI* and *COI*, especially at higher soiling levels. The value at $\lambda = 435$ nm, similar to the D&S-RGB, shows lower values than the other wavelengths, due to the lower spectral reflectance in that wavelength range. All correlations show good linear behavior though, permitting the use of the correlations to determine the target value, with slightly lower R^2 values, with a minimum 0.965, indicating slightly higher deviations from the linear behavior.

In Fig. 17, the data for the three wavelengths of the pFlex are displayed. The quality of the linear fit is similar to the other devices, with R^2 values above 0.99. Once again, the behavior of slightly lower reflectance values closer to the low wavelength range in which the reflectance declines can be recognized (at $\lambda = 535$ nm and $\lambda = 465$ nm).

As the CM700d gives values for the whole spectral range between 400 and 700 nm, only exemplary data is shown here. Selected are the values similar to D&S-15R and pFlex for comparison, that is $\lambda = \{460,$

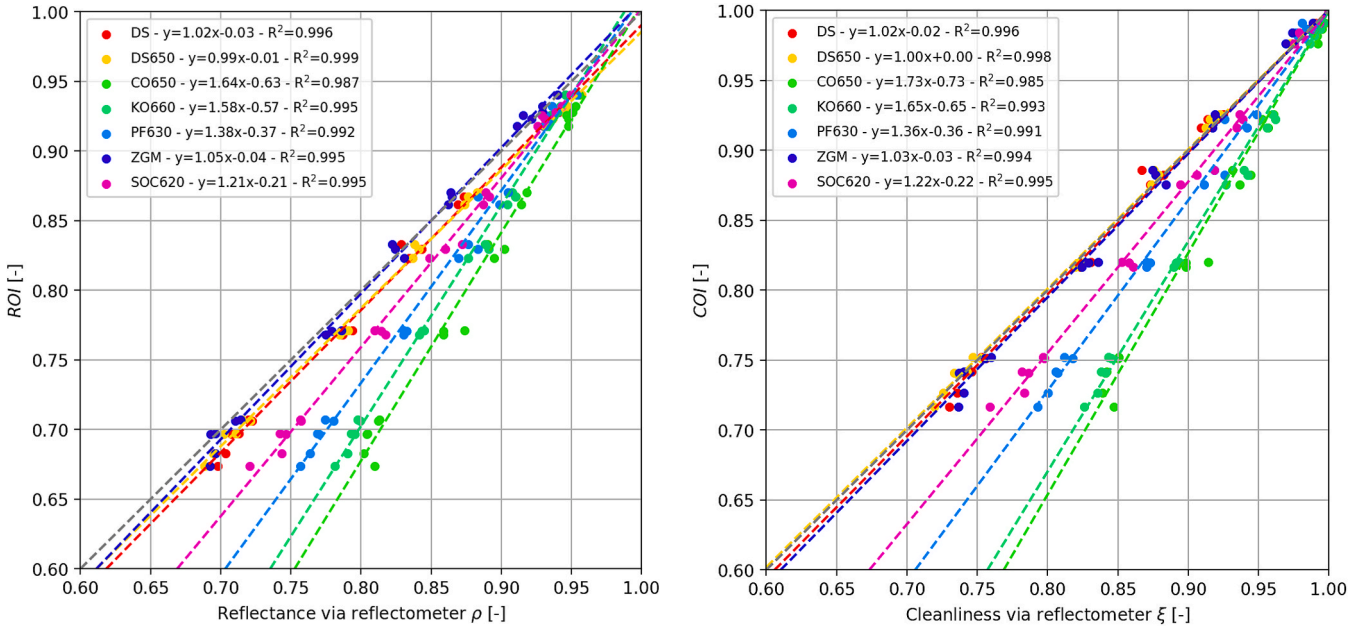

Fig. 14. Comparison of data from all reflectometers to the target value, red light source values where available (white for ZGM1130). Left: ROI, right: COI.

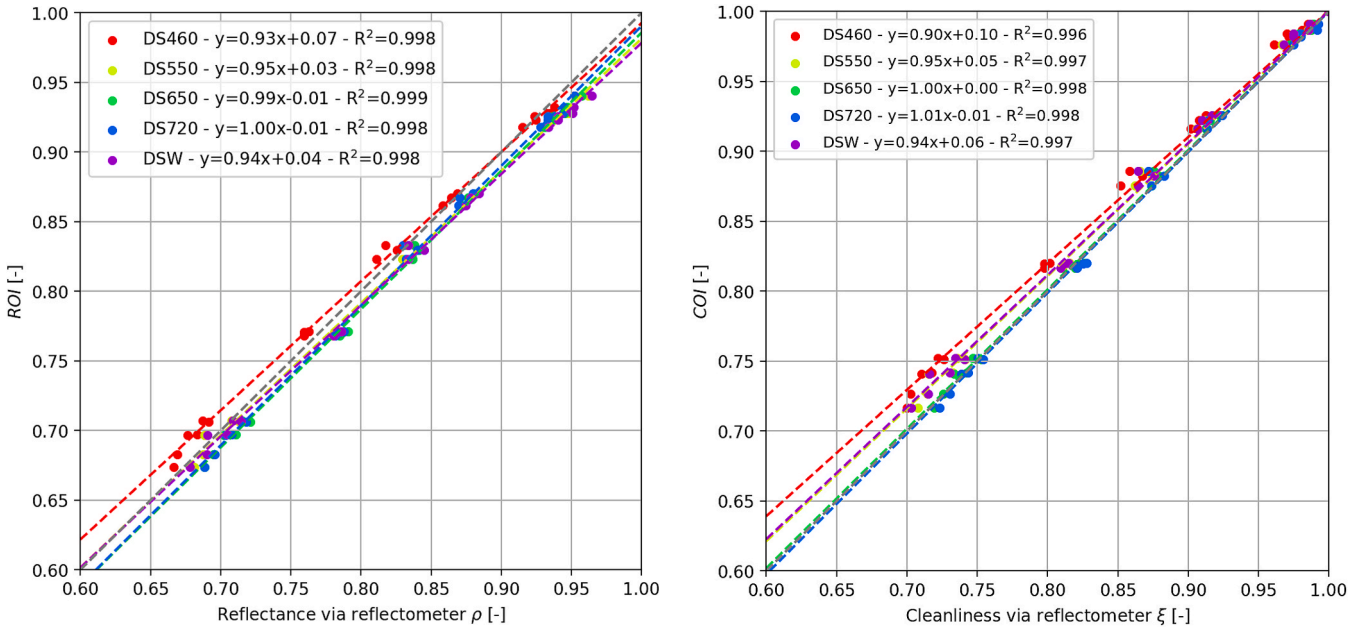

Fig. 15. D&S-RGB values for all wavelengths included, reflectance and cleanliness compared to the target values, ROI and COI.

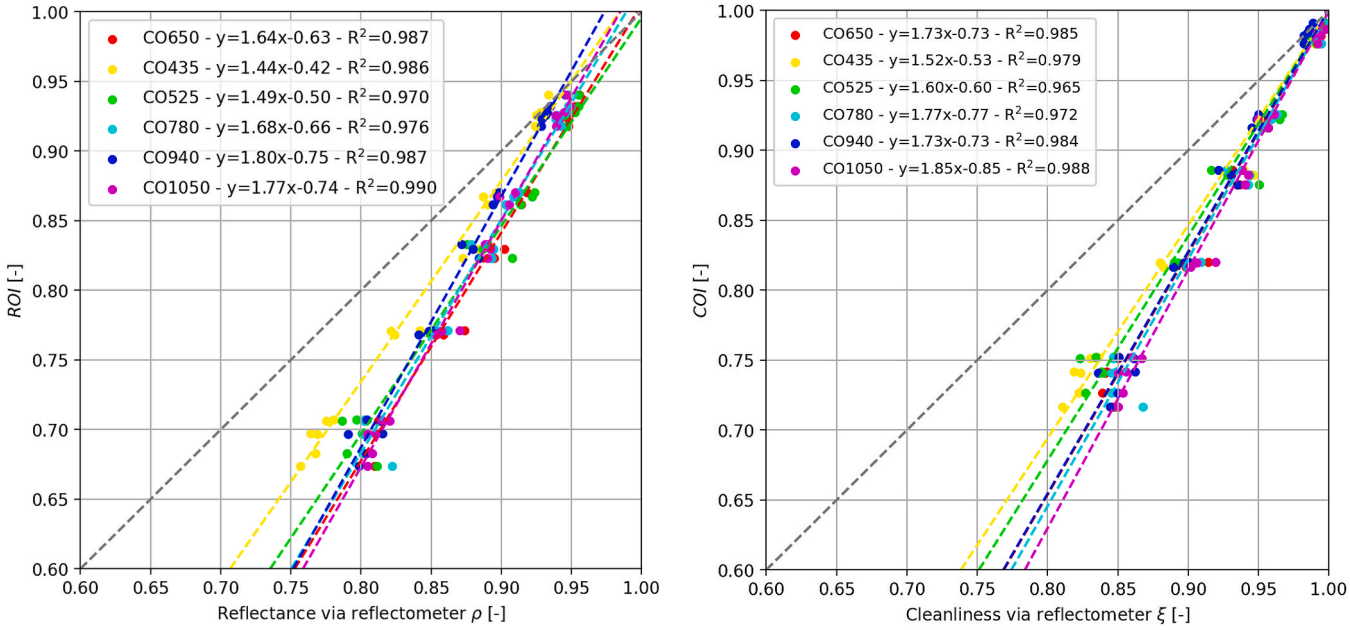

Fig. 16. Condor values for all wavelengths included, reflectance and cleanliness versus target values, ROI and COI.

530, 660} nm. Linear trend lines show good approximation, see Fig. 18. According to the results, the effective acceptance angle of the CM700d seems to lie higher than the pFlex one, but still considerably lower than the Condor value.

In Fig. 19, the data for the seven wavelengths of the SOC410 are plotted. Looking at the reflectance data (on the left), two groups of values can be distinguished: the two values at both ends of the spectrum (370 and 1820 nm) in contrast with the other values. These other values show similar behavior to the other reflectometers. At similar wavelengths, they show lower differences to the target value than the pFlex and CM700d, according to the lower acceptance angle of the SOC410. The two values at the ends of the spectrum lie in the range where stronger variations of the reflectance exist, which causes stronger differences to the target value. This can be explained by comparing the spectral reflectance data of the clean and soiled samples in Fig. 11 and Fig. 12. While the value at high wavelength ($\lambda = 1820$ nm) lies above the solar-weighted values for the clean sample and below for the soiled one, the reflectance at the low wavelength ($\lambda = 370$ nm) is considerably lower than the solar-weighted value for all soiling levels. Looking at the cleanliness, the influence of the lower spectral reflectance at low and high wavelengths decreases, and the behavior is more similar to the other equipment.

To show the influence of different incidence angles for the value of interest, the correlations to the other incidence angles for all reflectometers were calculated as well. The general behavior of robust linear correlation is the same as for the results presented above at 30° incidence. As the solar-weighted reflectance decreases with increasing incidence angle, and the reflectometers with higher acceptance angles

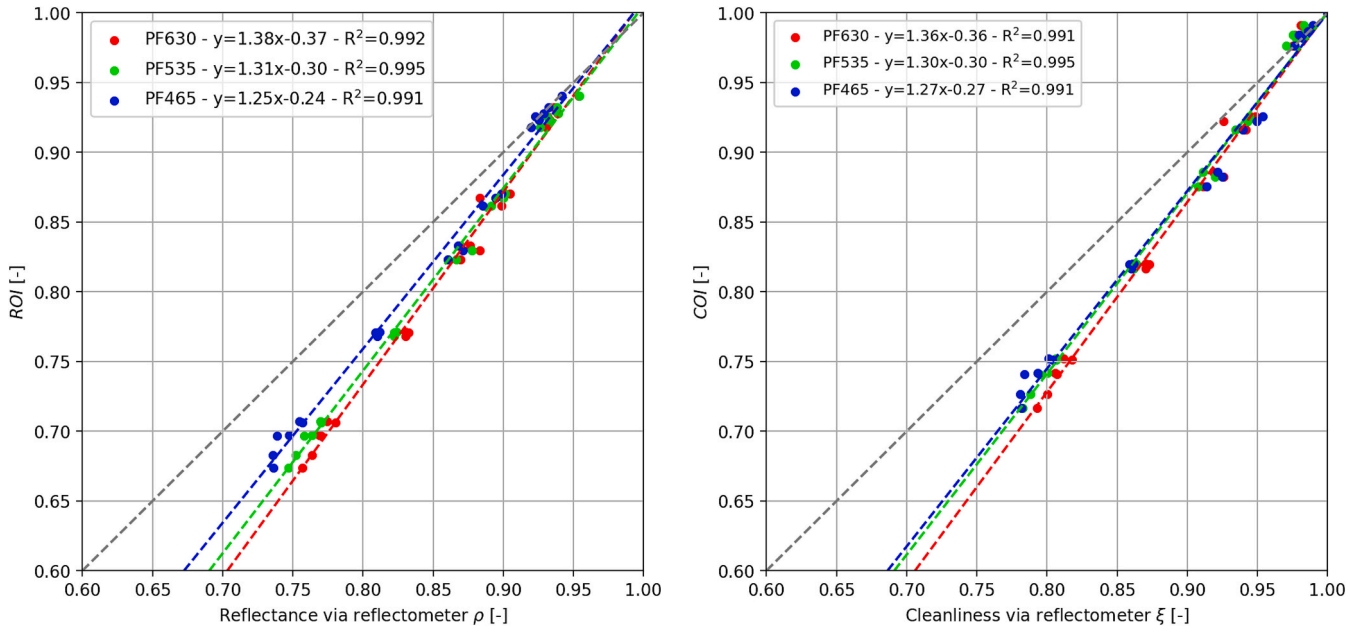

Fig. 17. pFlex values for all wavelengths included, reflectance and cleanliness over target values, ROI and COI.

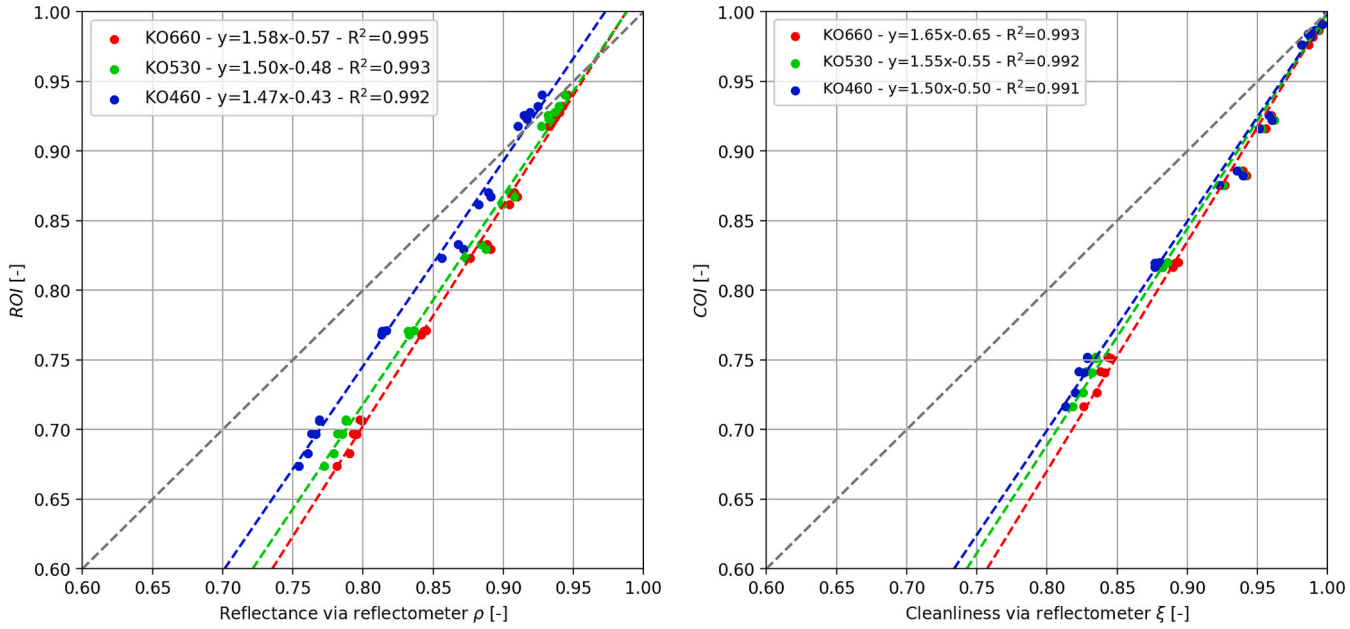

Fig. 18. CM700d values for three wavelengths, reflectance and cleanliness versus target values, ROI and COI.

usually show higher values than the S2R value, the differences also increase with the incidence angle. To illustrate this behavior, two examples are displayed in Fig. 20, including the three measured incidence angles. On the left the data for the D&S-15R with the smallest acceptance angle and on the right for the Condor (at the same wavelength as D&S-15R) with the highest acceptance angle are displayed. Differences are rather small for target values with 15° and 30° incidence, but stronger differences can be seen for 60°, especially at higher soiling levels.

The full dataset for all linear correlations of all target incidence angles and all reflectometer wavelengths can be consulted in the appendix for the reflectance and cleanliness.

3.6. Comparison of correlations to results from past campaigns

Several questions remain to be addressed concerning the validity of the correlations between measurement devices and parameters. For example, in the past the question on the influence of the type of soiling on the reflectance was raised. Depending on the size and composition of the particles, and the way they adhered to the surface (e.g. involving dry or humid conditions, different heterogeneous soiling pattern formation), the absorption and scattering may change and thus influence acceptance-angle- and wavelength-dependent behavior [53]. In principle, this limits the use of the correlations to the PSA for which they were developed.

To gain experience on the universality of the correlations found here, the values of this work were compared to previously published data. In the following paragraph, data from three publications, involving

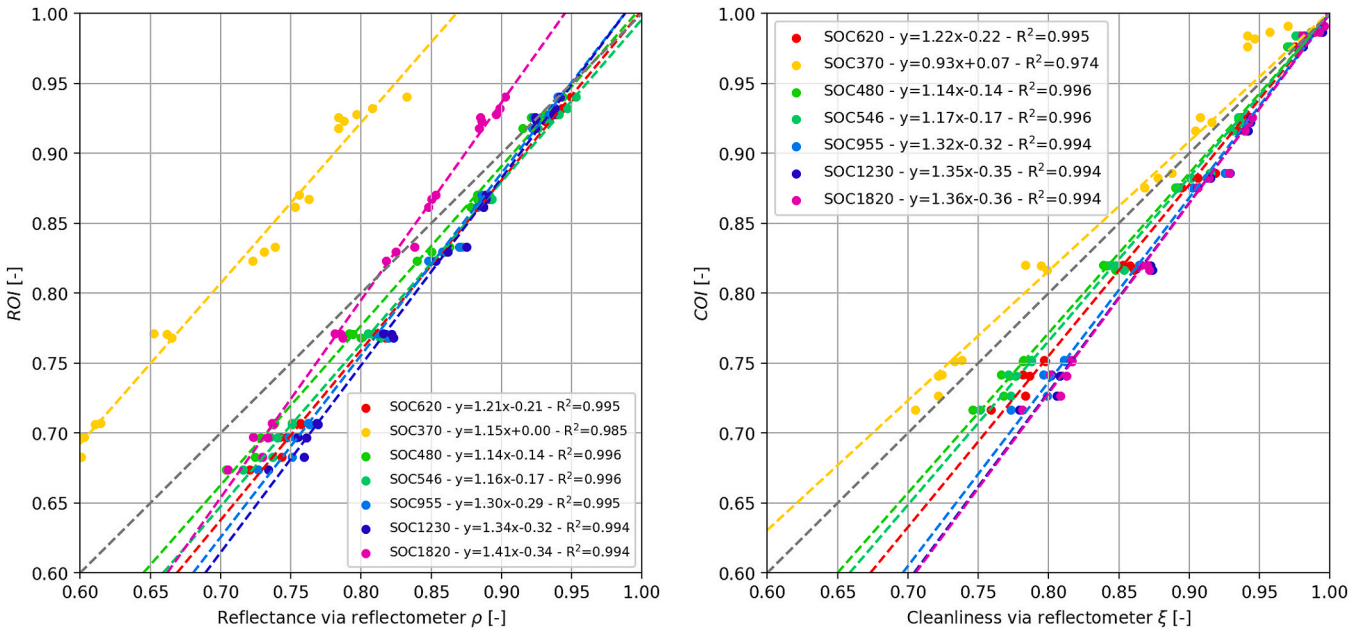

Fig. 19. SOC410 values, all wavelengths, reflectance and cleanliness versus target values, ROI and COI.

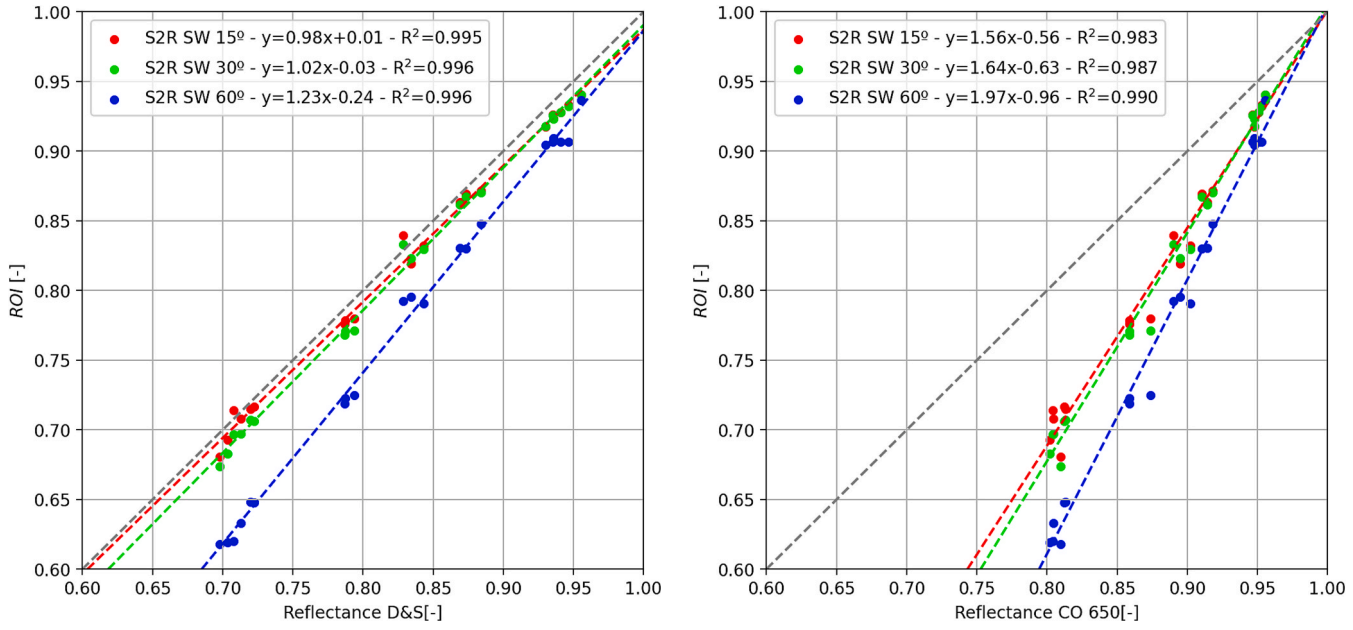

Fig. 20. One reflectometer vs. ROI at three incidence angles (S2R), left: D&S-15R, right: Condor – 650 nm.

combinations of the same devices used for this study, are compared to this data. All of these references used soiling measurements on the same type of material (namely 4 mm silvered-glass reflectors). These previous studies do not include the here used *ROI/COI* values, and thus only allow evaluation of the direct comparison of the portable devices in question.

Sansom et al. [50] conducted an outdoor measurement campaign at the PSA in 2015. The D&S-15R and the Condor device were included in the study. During a three-week period, measurements were taken on three facets of a PTC, with five measurements per facet. The publication includes a direct comparison of the reflectance of the two devices, taking the 650 nm value for the Condor. A linear correlation was found with the following parameters $\rho_{D\&S} = 1.782^{*}\rho_{Condor}$-0.741. The same comparison is performed with the data from the here presented study and is displayed in Fig. 21. The resulting equation for this experiment is $\rho_{D\&S} = 1.6^{*}\rho_{Condor}$-0.59, which is in reasonable agreement with the other campaign. This agreement indicates that soiling form different seasons only has a limited influence on the correlations. The trend line and covered reflectance range are marked in blue in the figure. The data of the 2015 campaign shows much more scattering, resulting in a lower R^2 value of 0.752, compared to a value of $R^2 = 0.991$ for this campaign. This scattering may also explain the differences in the values of the linear trend lines. Absolute differences from the linear trend exceed 3 % pt of reflectance for some of the data points. Causes of the high scattering may be the fact that outdoor measurements are performed and, above all, that measurements are not taken on the same measurement spots with the two devices, but mean values of whole-facet measurements are taken into account. In addition, the soiling range for the first study is limited to reflectance values over 0.860, while much lower reflectance values (minimum 0.7) are included for the current one.

A similar campaign was published by Crawford et al. [52] in 2012.

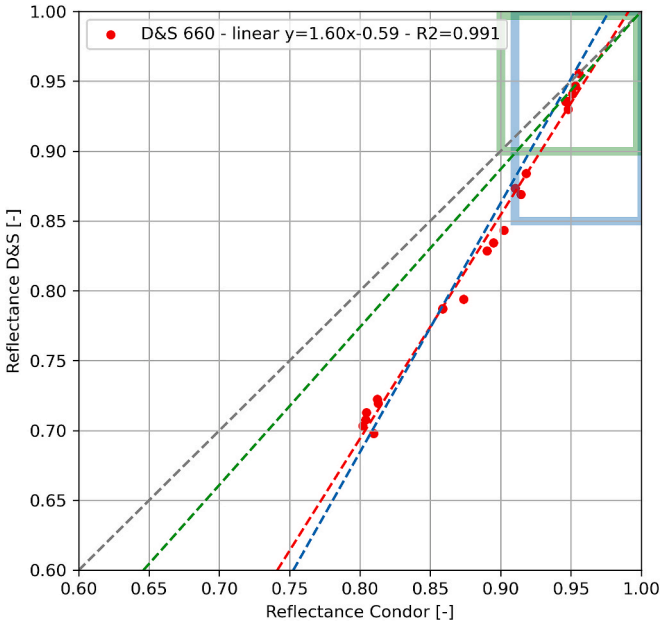

Fig. 21. Reflectance of the Condor at 650 nm versus the D&S-15R values, data points of actual campaign in red, covered ranges and trend lines from previous studies marked in blue [50] and green [52].

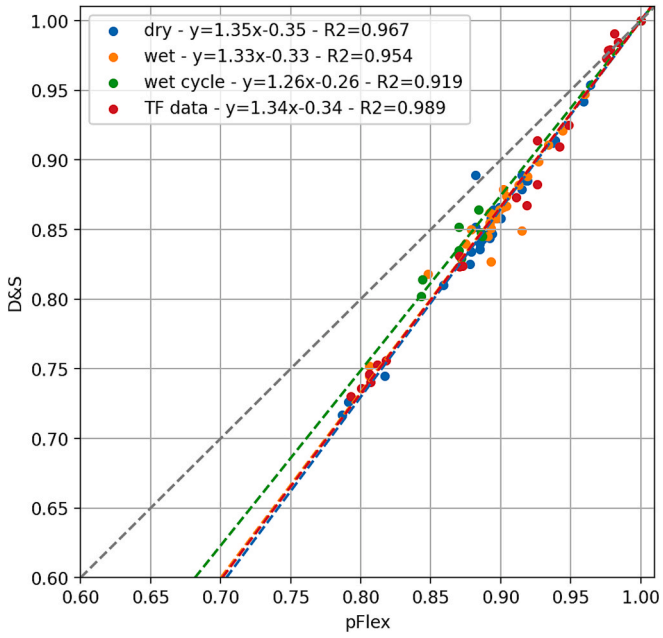

Fig. 22. Measurement data from [11], including three campaigns and the present campaign, cleanliness data from pFlex versus D&S-15R together with corresponding linear trend lines.

Here, measurements from D&S-15R, Condor and SOC410 were performed on a PTC in Lakewood, USA during six months. The SOC410 measurements showed inconclusive results and the hypothesis of facet thickness and curvature influence was raised. This could point to a similar issue as for the device in this study, which was addressed here with the designed adapter. The comparison of Condor and D&S-15R reflectance values resulted in a linear approximation with the following parameters: $\rho_{D\&S} = 1.13*\rho_{Condor}$-0.13. Here the resulting R^2 was 0.81. The slope of the equation here is much lower than for the other data, which indicates a lower influence of the acceptance angle. The included soiling range for this study is even lower than for the one presented before, with minimum values of reflectance around $\rho_{D\&S} = 0.9$. Covered reflectance range and resulting trend line from the study are included in Fig. 21 in green. Even though much lower cleanliness values are usually avoided during commercial operation, for the determination of the correlations, it may be beneficial to include low cleanliness values, to improve the precision of the calculation of the slope. This is especially recommended when scattering of data is high. It is not possible to decide at this point whether differences in the correlations between studies stem from the high scattering and low covered range or are due to other factors, such as the potentially different soiling types.

A recent study was performed by Anderson et al. [51], in which artificial soiling was used and the impact of dry and condensation conditions was evaluated. Natural dust from a site in Mount Isa, Australia, was employed to artificially soil reflector samples under laboratory conditions. Several techniques were applied to determine the soiling impact, including reflectance measurements with the D&S-15R and the pFlex (at $\lambda = 630$ nm). In Fig. 22, the data for these two devices are displayed for three conducted campaigns of this study ("dry, wet, and wet cycle"), together with the data from the present campaign. Excellent agreement between both studies is found with very similar equation parameters, with near-perfect match e.g. of the cited "dry" campaign of $\rho_{pFlex} = 1.35*\rho_{D\&S}$-0.35 in comparison to $\rho_{pFlex} = 1.34*\rho_{D\&S}$-0.34 for the actual campaign. Values for the "wet" campaign are equally good, and slight differences exist with the "wet cycle" conditions. R^2 are still high for the cited campaigns with a minimum value of 0.919 for the "wet cycle" case due to more scattering of the data. The very good agreement shows that the difference in soiling type, from two different sites (Almería and Mount Isa), does not have a significant impact on the validity of the found correlations between the portable reflectometers in this case. It is strongly recommended to include *ROI/COI* measurements from different sites in future campaigns to further investigate the complex influence of soiling type on cleanliness.

4. Conclusions

Linear correlations between the readings determined with a portable reflectometer and the target values of interest (i.e., the solar specular reflectance and the cleanliness measured at the typical incidence and acceptance angle of the given plant) were found for all commercial reflectometers and corresponding wavelengths included in this study. This allows for the translation of the reflectometer readings to the much more significant values *ROI* and *COI*. Such a translation requires determining the linear coefficients between reading values of the adopted reflectometer and the results obtained with an instrument suitable for measuring the reflectance at the incidence and acceptance angles of interest of the given plant, such as the S2R. This results in benefits for various stakeholders of CST applications. Plant owners and operators can improve their cleaning strategies, as well as yield calculation and prediction. It can also facilitate a better intercomparison of various sites. For researchers and developers, advantages lie in the possibility of comparing measurement campaigns, validate methods for different sites and develop advanced soiling models. It was shown that, without the use of correlations, the readings of the devices with lower acceptance angles show smaller variations to the target values, *ROI* and *COI,* due to the similarity in the acceptance angle.

The correlations were developed using soiling at one specific site. Additional data was included for several direct reflectometer comparisons, without *ROI* measurements available. Two seasons at the studied site were compared without variations in the correlations, which indicates an insignificant seasonal influence. Very good agreement was found for a previously published study with a different soiling type, which indicates a low dependence of the direct correlation between reflectometers on the soiling type. Former works had implied that the correlations are highly site-specific, though. This is why investigations on the validity of the correlation are recommended for further sites and especially including *ROI* measurements.

The methodology presented in this work may serve to establish additional correlations for different sites and values of interest. Experience from this campaign leads to two main recommendations for determining the correlations. Firstly, due to the inherent heterogeneity of soiling, measurements from the same spots on samples or facets should be compared. Alternatively, a high number of measurements could be used to ensure representative mean values. Secondly, including a wider range of cleanliness values (cleaner and more soiled material) may benefit the quality of the correlations.

The important range of incidence angles for CST technologies is covered here, but for the acceptance angle the investigation was limited to the most significant mean value. If other acceptance angles are of interest, correlations should be adapted. Also, a further evaluation of the influence on the time-dependent local acceptance angle is recommended for future studies.

CRediT authorship contribution statement

Johannes Wette: Writing – original draft, Visualization, Investigation, Conceptualization. **Florian Sutter:** Writing – review & editing, Validation, Supervision, Conceptualization. **Teresa Diamantino:** Writing – review & editing, Validation, Methodology, Data curation. **Marco Montecchi:** Writing – review & editing, Validation, Methodology, Conceptualization. **Gregor Bern:** Writing – review & editing, Validation, Methodology, Conceptualization. **Aránzazu Fernández-García:** Writing – original draft, Validation, Supervision, Methodology, Investigation, Conceptualization.

Declaration of competing interest

The authors declare that they have no known competing financial interests or personal relationships that could have appeared to influence the work reported in this paper.

Acknowledgements

The work for this study was conducted during the project *Update of guideline "Recommendations for reflectance measurements on soiled solar mirrors"* funded by SolarPACES, a Technology Collaboration Programme (TCP) of the International Energy Agency (IEA), within the task Task III: "Solar Technology and Advanced Applications".

Appendix

Tables correlation functions.

Table A1
Correlation coefficients of D&S-15R to ROI/COI.

Value of interest	Reflectometer	[nm]	Linear equation		
			a	*b*	R^2
ROI (15°, 12.5mrad)	D&S-15R	660	0.977	0.01	0.995
ROI (30°, 12.5mrad)			1.023	−0.033	0.996
ROI (60°, 12.5mrad)			1.227	−0.241	0.996
COI (15°, 12.5mrad)			0.975	0.026	0.994
COI (30°, 12.5mrad)			1.016	−0.016	0.996
COI (60°, 12.5mrad)			1.274	−0.274	0.996

Table A2
Correlation coefficients of D&S-RGB, all wavelengths, to ROI/COI.

Value of interest	Reflectometer	[nm]	Linear equation		
			a	*b*	R^2
ROI (15°, 12.5mrad)	D&S-RGB	460	0.885	0.104	0.997
		550	0.907	0.072	0.996
		650	0.948	0.035	0.997
		720	0.958	0.029	0.996
		white	0.899	0.076	0.996
ROI (30°, 12.5mrad)		460	0.927	0.065	0.998
		550	0.95	0.032	0.998
		650	0.993	−0.007	0.999
		720	1.004	−0.013	0.998
		white	0.942	0.036	0.998
ROI (60°, 12.5mrad)		460	1.111	−0.122	0.996
		550	1.138	−0.163	0.997
		650	1.19	−0.209	0.997
		720	1.203	−0.216	0.996
		white	1.129	−0.157	0.997
COI (15°, 12.5mrad)		460	0.867	0.133	0.995
		550	0.909	0.091	0.995
		650	0.955	0.045	0.997
		720	0.965	0.035	0.996
		white	0.906	0.095	0.995
COI (30°, 12.5mrad)		460	0.904	0.097	0.996
		550	0.948	0.053	0.997
		650	0.996	0.005	0.998
		720	1.006	−0.006	0.998
		white	0.944	0.056	0.997

(*continued on next page*)

Table A2 (*continued*)

Value of interest	Reflectometer	[nm]	Linear equation		
			a	*b*	R^2
COI (60°, 12.5mrad)		460	1.133	−0.133	0.996
		550	1.188	−0.188	0.996
		650	1.248	−0.248	0.996
		720	1.261	−0.261	0.995
		white	1.183	−0.184	0.996

Table A3
Correlation coefficients of Condor, all wavelengths, to ROI/COI.

Value of interest	Reflectometer	[nm]	Linear equation		
			a	*b*	R^2
ROI (15°, 12.5mrad)	Condor	435	1.374	−0.356	0.983
		525	1.423	−0.431	0.963
		650	1.563	−0.562	0.983
		780	1.595	−0.582	0.969
		940	1.717	−0.676	0.982
		1050	1.688	−0.666	0.987
ROI (30°, 12.5mrad)		435	1.44	−0.418	0.986
		525	1.495	−0.499	0.97
		650	1.639	−0.634	0.987
		780	1.675	−0.657	0.976
		940	1.802	−0.754	0.987
		1050	1.769	−0.742	0.99
ROI (60°, 12.5mrad)		435	1.725	−0.701	0.984
		525	1.795	−0.802	0.973
		650	1.967	−0.963	0.99
		780	2.013	−0.993	0.98
		940	2.166	−1.111	0.992
		1050	2.123	−1.093	0.991
COI (15°, 12.5mrad)		435	1.461	−0.463	0.975
		525	1.536	−0.537	0.957
		650	1.657	−0.657	0.981
		780	1.695	−0.696	0.965
		940	1.66	−0.659	0.98
		1050	1.772	−0.773	0.984
COI (30°, 12.5mrad)		435	1.524	−0.525	0.979
		525	1.604	−0.605	0.965
		650	1.728	−0.728	0.985
		780	1.768	−0.769	0.972
		940	1.731	−0.73	0.984
		1050	1.848	−0.848	0.988
COI (60°, 12.5mrad)		435	1.906	−0.908	0.965
		525	2.008	−1.01	0.958
		650	2.164	−1.166	0.98
		780	2.216	−1.218	0.968
		940	2.174	−1.174	0.992
		1050	2.314	−1.315	0.982

Table A4
Correlation coefficients of pFlex, all wavelengths, to ROI/COI.

Value of interest	Reflectometer	[nm]	Linear equation		
			a	*b*	R^2
ROI (15°, 12.5mrad)	pFlex	465	1.189	−0.185	0.987
		535	1.249	−0.247	0.993
		630	1.318	−0.312	0.99
ROI (30°, 12.5mrad)		465	1.247	−0.239	0.991
		535	1.308	−0.303	0.995
		630	1.38	−0.371	0.992
ROI (60°, 12.5mrad)		465	1.495	−0.487	0.99
		535	1.568	−0.564	0.994
		630	1.656	−0.646	0.992
COI (15°, 12.5mrad)		465	1.222	−0.222	0.986
		535	1.243	−0.243	0.992
		630	1.306	−0.306	0.989
COI (30°, 12.5mrad)		465	1.274	−0.274	0.991
		535	1.296	−0.296	0.995
		630	1.362	−0.361	0.991
COI (60°, 12.5mrad)		465	1.596	−0.597	0.984

(*continued on next page*)

Table A4 (*continued*)

Value of interest	Reflectometer	[nm]	Linear equation		
			a	*b*	R^2
		535	1.625	−0.625	0.993
		630	1.707	−0.708	0.992

Table A5
Correlation coefficients of CM700d, all wavelengths, to ROI/COI.

Value of interest	Reflectometer	[nm]	Linear equation		
			a	*b*	R^2
ROI (15°, 12.5mrad)	CM700d	460	1.407	−0.372	0.99
		530	1.432	−0.418	0.991
		660	1.513	−0.498	0.994
ROI (30°, 12.5mrad)		460	1.474	−0.434	0.992
		530	1.5	−0.482	0.993
		660	1.584	−0.565	0.995
ROI (60°, 12.5mrad)		460	1.764	−0.718	0.987
		530	1.795	−0.776	0.988
		660	1.895	−0.875	0.99
COI (15°, 12.5mrad)		460	1.439	−0.439	0.988
		530	1.49	−0.49	0.989
		660	1.579	−0.579	0.991
COI (30°, 12.5mrad)		460	1.5	−0.501	0.991
		530	1.553	−0.554	0.992
		660	1.646	−0.646	0.993
COI (60°, 12.5mrad)		460	1.877	−0.878	0.979
		530	1.943	−0.944	0.98
		660	2.058	−1.06	0.981

Table A6
Correlation coefficients of SOC410, all wavelengths, to ROI/COI.

Value of interest	Reflectometer	[nm]	Linear equation		
			a	*b*	R^2
ROI (15°, 12.5mrad)	SOC410	370	1.096	0.045	0.982
		480	1.089	−0.088	0.995
		546	1.109	−0.117	0.995
		620	1.161	−0.162	0.996
		955	1.244	−0.232	0.995
		1230	1.279	−0.267	0.994
		1820	1.35	−0.28	0.995
ROI (30°, 12.5mrad)		370	1.149	0.003	0.985
		480	1.14	−0.135	0.996
		546	1.161	−0.165	0.996
		620	1.215	−0.212	0.995
		955	1.301	−0.285	0.995
		1230	1.338	−0.322	0.994
		1820	1.413	−0.335	0.994
ROI (60°, 12.5mrad)		370	1.376	−0.197	0.983
		480	1.364	−0.361	0.99
		546	1.389	−0.396	0.99
		620	1.452	−0.453	0.99
		955	1.556	−0.54	0.988
		1230	1.6	−0.583	0.988
		1820	1.689	−0.599	0.988
COI (15°, 12.5mrad)		370	0.889	0.112	0.972
		480	1.096	−0.097	0.995
		546	1.124	−0.124	0.995
		620	1.175	−0.175	0.996
		955	1.263	−0.264	0.995
		1230	1.298	−0.298	0.994
		1820	1.303	−0.303	0.995
COI (30°, 12.5mrad)		370	0.926	0.075	0.974
		480	1.143	−0.143	0.996
		546	1.172	−0.172	0.996
		620	1.225	−0.225	0.995
		955	1.316	−0.317	0.994
		1230	1.353	−0.353	0.994
		1820	1.358	−0.358	0.994
COI (60°, 12.5mrad)		370	1.163	−0.162	0.979
		480	1.43	−0.431	0.988

(*continued on next page*)

Table A6 (*continued*)

Value of interest	Reflectometer	[nm]	Linear equation		
			a	*b*	R^2
		546	1.467	−0.467	0.988
		620	1.533	−0.533	0.987
		955	1.647	−0.648	0.984
		1230	1.692	−0.693	0.984
		1820	1.699	−0.7	0.985

Table A7
Correlation coefficients of ZGM1130 to ROI/COI.

Value of interest	Reflectometer	[nm]	Linear equation		
			a	*b*	R^2
ROI (15°, 12.5mrad)	ZGM1130	white	1	0.003	0.992
ROI (30°, 12.5mrad)			1.048	−0.041	0.995
ROI (60°, 12.5mrad)			1.257	−0.251	0.996
COI (15°, 12.5mrad)			0.985	0.015	0.991
COI (30°, 12.5mrad)			1.027	−0.027	0.994
COI (60°, 12.5mrad)			1.288	−0.288	0.995

References

[1] M.I. Khan, R. Gutiérrez-Alvarez, F. Asfand, Y. Bicer, S. Sgouridis, S.G. Al-Ghamdi, H. Jouhara, M. Asif, T.A. Kurniawan, M. Abid, A. Pesyridis, M. Farooq, The economics of concentrating solar power (CSP): Assessing cost competitiveness and deployment potential, Renew. Sustain. Energy Rev. 200 (2024) 114551, https://doi.org/10.1016/j.rser.2024.114551.

[2] F. Schöniger, R. Thonig, G. Resch, J. Lilliestam, Making the sun shine at night: comparing the cost of dispatchable concentrating solar power and photovoltaics with storage, Energy Source. 16 (2021) 20, https://doi.org/10.1080/15567249.2020.1843565.

[3] O. Ališauskas, World Energy Outlook 2024, IEA, 2024.

[4] Global Renewables Outlook: Energy Transformation 2050, IRENA, Abu Dhabi, 2020.

[5] X. Xiao, J. Wang, D.J. Hill, Impact of Large-scale concentrated solar power on energy and auxiliary markets, Appl. Energy 318 (2022) 119216, https://doi.org/10.1016/j.apenergy.2022.119216.

[6] A. García-Segura, F. Sutter, L. Martínez-Arcos, T.J. Reche-Navarro, F. Wiesinger, J. Wette, F. Buendía-Martínez, A. Fernández-García, Degradation types of reflector materials used in concentrating solar thermal systems, Renew. Sustain. Energy Rev. 143 (2021) 110879, https://doi.org/10.1016/j.rser.2021.110879.

[7] F. Buendía-Martínez, F. Sutter, J. Wette, L. Valenzuela, A. Fernández-García, Lifetime prediction model of reflector materials for concentrating solar thermal energies in corrosive environments, Sol. Energy Mater. Sol. Cells 224 (2021) 110996, https://doi.org/10.1016/j.solmat.2021.110996.

[8] F. Wiesinger, F. Sutter, A. Fernández-García, J. Reinhold, R. Pitz-Paal, Sand erosion on solar reflectors: Accelerated simulation and comparison with field data, Sol. Energy Mater. Sol. Cells 145 (2016) 303–313, https://doi.org/10.1016/j.solmat.2015.10.036.

[9] C. Sansom, P. Comley, D. Bhattacharyya, N. Macerol, A Comparison of Polymer Film and Glass collectors for Concentrating Solar Power, Energy Procedia 49 (2014) 209–219, https://doi.org/10.1016/j.egypro.2014.03.023.

[10] R. Sánchez-Moreno, F. Buendía-Martínez, A. Fernández-García, J. Wette, F. Sutter, Degradation of primary mirrors under accelerating aging tests, AIP Conf. Proc. 2815 (2023) 020016, https://doi.org/10.1063/5.0149842.

[11] O. Raccurt, C. Delord, C. Bouquet, R. Couturier, Correlation between Solar Mirror Degradation and Colorimetric Measurement of protective Back Layer, Energy Procedia 49 (2013) 1700–1707, https://doi.org/10.1016/j.egypro.2014.03.179.

[12] T. Farrell, Y. Cao, F. Burkholder, D. Celvi, C. Schreiber, G. Zhu, Compilation of a Solar Mirror Materials Database and an Analysis of Natural and Accelerated Mirror Exposure and Degradation, J. Sol. Energy Eng. 145 (2023), https://doi.org/10.1115/1.4063079.

[13] C. Kennedy, Advances in Reflector and Solar Selective Materials for Application to Concentrating Solar Power Systems, in: Montecatini Terme, Italy, 2010.

[14] G. Gug Jang, D. Barton Smith, G. Polizos, L. Collins, J.K. Keum, D.F. Lee, Transparent superhydrophilic and superhydrophobic nanoparticle textured coatings: comparative study of anti-soiling performance, Nanoscale Advances 1 (2019) 1249–1260, https://doi.org/10.1039/C8NA00349A.

[15] J. Wette, F. Sutter, A. Fernández-García, Evaluation of anti-soiling coatings for CSP reflectors under realistic outdoor conditions, Sol. Energy 191 (2019) 574–584, https://doi.org/10.1016/j.solener.2019.09.031.

[16] V.L. Morris, Cleaning agents and techniques for concentrating solar collectors, Sol. Energy Mater. 3 (1980) 35–55, https://doi.org/10.1016/0165-1633(80)90048-9.

[17] A. Fernández-García, L. Álvarez-Rodrigo, L. Martínez-Arcos, R. Aguiar, J. M. Márquez-Payés, Study of different cleaning Methods for Solar Reflectors used in CSP Plants, Energy Procedia 49 (2014) 80–89, https://doi.org/10.1016/j.egypro.2014.03.009.

[18] S. Benyadry, M. Halimi, A. Khouya, Soiling impact and cleaning techniques for optimizing photovoltaic and concentrated solar power power production: a state-of-the-art review, Energy Environ. (2024) 1–33, https://doi.org/10.1177/0958305X241230624.

[19] K. Zereg, A. Gama, M. Aksas, N. Rathore, F. Yettou, N. Lal Panwar, Dust impact on concentrated solar power: a review, Environ. Eng. Res. 27 (2021) 210345, https://doi.org/10.4491/eer.2021.345.

[20] R. Levinson, H. Akbari, P. Berdahl, Measuring solar reflectance—Part II: Review of practical methods, Sol. Energy 84 (2010) 1745–1759, https://doi.org/10.1016/j.solener.2010.04.017.

[21] H. Wang, W. Zhang, A. Dong, Measurement and modeling of Bidirectional Reflectance distribution Function (BRDF) on material surface, Measurement 46 (2013) 3654–3661, https://doi.org/10.1016/j.measurement.2013.07.008.

[22] A. Fernandez-Garcia, F. Sutter, M. Montecchi, F. Sallaberry, A. Heimath, C. Heras, E. Le Baron, A. Soum-Glaude, Parameters and Method to Evaluate the Reflectance Properties of Reflector Materials for Concentrating Solar Power Technology Technology - Official Reflectance Guideline Version 3.1, SolarPACES (2020).

[23] M. Montecchi, Proposal of a new parameter for the comprehensive qualification of solar mirrors for CSP applications, AIP Conf. Proc. 1734 (2016) 130014, https://doi.org/10.1063/1.4949224.

[24] IEC 60904-3:2019. Photovoltaic devices – Part 3: Measurement principles for terrestrial photovoltaic (PV) solar devices with reference spectral irradiance data, (2019). https://webstore.iec.ch/en/publication/61084 (accessed March 6, 2025).

[25] R. B. PETTIT, J. M. FREESE, WAVELENGTH DEPENDENT SCATTERING CAUSED BY DUST ACCUMULATION ON SOLAR MIRRORS, (1980).

[26] Stephanie Meyen, Eckhard Lüpfert, Aránzazu Fernández-García, Cheryl Kennedy, Standardization of Solar Mirror Reflectance Measurements – Round Robin Test, (2010).

[27] F. Sutter, M. Montecchi, H. von Dahlen, A. Fernández-García, M. Röger, The effect of incidence angle on the reflectance of solar mirrors, Sol. Energy Mater. Sol. Cells 176 (2018) 119–133, https://doi.org/10.1016/j.solmat.2017.11.029.

[28] A. Heimsath, P. Nitz, The effect of soiling on the reflectance of solar reflector materials - Model for prediction of incidence angle dependent reflectance and attenuation due to dust deposition, Sol. Energy Mater. Sol. Cells 195 (2019) 258–268, https://doi.org/10.1016/j.solmat.2019.03.015.

[29] A. Fernández-García, F. Sutter, L. Martínez-Arcos, C. Sansom, F. Wolfertstetter, C. Delord, Equipment and methods for measuring reflectance of concentrating solar reflector materials, Sol. Energy Mater. Sol. Cells 167 (2017) 28–52, https://doi.org/10.1016/j.solmat.2017.03.036.

[30] F. Sutter, S. Meyen, A. Fernández-García, P. Heller, Spectral characterization of specular reflectance of solar mirrors, Sol. Energy Mater. Sol. Cells 145 (2016) 248–254, https://doi.org/10.1016/j.solmat.2015.10.030.

[31] F. Sutter, A. Fernández-García, A. Heimsath, M. Montecchi, C. Pelayo, Advanced measurement techniques to characterize the near-specular reflectance of solar mirrors, AIP Conf. Proc. 2126 (2019) 110003, https://doi.org/10.1063/1.5117618.

[32] J. Wette, F. Sutter, R. Sánchez-Moreno, A. Fernández-García, Comparison of Commercial Reflectometers for Solar Mirrors, SolarPACES Conference Proceedings 1 (2022). https://doi.org/10.52825/solarpaces.v1i.666.

[33] A. Alami Merrouni, R. Conceição, A. Mouaky, H.G. Silva, A. Ghennioui, CSP performance and yield analysis including soiling measurements for Morocco and Portugal, Renewable Energy 162 (2020) 1777–1792, https://doi.org/10.1016/j.renene.2020.10.014.

[34] S. Rohani, N. Abdelnabi, T. Fluri, A. Heimsath, C. Wittwer, J. Ainsua, Optimized mirror cleaning strategies in PTC plants reducing the water consumption and the levelized cost of cleaning, AIP Conf. Proc. 2126 (2019) 220004, https://doi.org/10.1063/1.5117763.
[35] F. Wolfertstetter, S. Wilbert, J. Dersch, S. Dieckmann, R. Pitz-Paal, A. Ghennioui, Integration of Soiling-Rate Measurements and cleaning strategies in Yield Analysis of Parabolic Trough Plants, J. Sol. Energy Eng. 140 (2018), https://doi.org/10.1115/1.4039631.
[36] G. Zhu, D. Kearney, M. Mehos, On characterization and measurement of average solar field mirror reflectance in utility-scale concentrating solar power plants, Sol. Energy 99 (2014) 185–202, https://doi.org/10.1016/j.solener.2013.11.009.
[37] J. Fernández-Reche, Reflectance measurement in solar tower heliostats fields, Sol. Energy 80 (2006) 779–786, https://doi.org/10.1016/j.solener.2005.06.006.
[38] A.M. Bonanos, A.C. Montenon, M.J. Blanco, Estimation of mean field reflectance in CST applications, Sol. Energy 208 (2020) 1031–1038, https://doi.org/10.1016/j.solener.2020.08.073.
[39] A. Heimsath, T. Schmidt, J. Steinmetz, C. Reetz, M. Schwandt, R. Meyer, P. Nitz, Automated monitoring of soiling with AVUS instrument for improved solar site assessment, in: Santiago, Chile, 2018: p. 190008. https://doi.org/10.1063/1.5067193.
[40] F. Wolfertstetter, N. Hanrieder, P. Bellmann, A. Ghennioui, J. Wette, A. Fernandez-Garcia, Parallel soiling measurements for 4 mirror samples during outdoor exposure with TraCS, AIP Conf. Proc. 2303 (2020) 100009, https://doi.org/10.1063/5.0028969.
[41] M. Gostein, S. Faullin, K. Miller, J. Schneider, B. Stueve, Mars Soiling Sensor™, in: 2018 IEEE 7th World Conference on Photovoltaic Energy Conversion (WCPEC) (A Joint Conference of 45th IEEE PVSC, 28th PVSEC & 34th EU PVSEC), IEEE, Waikoloa Village, HI, 2018: pp. 3417–3420. https://doi.org/10.1109/PVSC.2018.8547767.
[42] M. Tian, N. Desai, J. Bai, R. Brost, D. Small, D. Novick, J. Yellowhair, M.Z. E. Rafique, V. Pisharam, Y. Yao, Toward Autonomous Field Inspection of CSP collectors with a Polarimetric Imaging Drone, SolarPACES Conf Proc 1 (2023). https://doi.org/10.52825/solarpaces.v1i.623.
[43] J. Coventry, C.-A. Asselineau, E. Salahat, M.A. Raman, R. Mahony, A robotic vision system for inspection of soiling at CSP plants, in: Daegu, South Korea, 2020: p. 100001. https://doi.org/10.1063/5.0029493.
[44] F. Wolfertstetter, R. Fonk, C. Prahl, M. Röger, S. Wilbert, J. Fernández-Reche, Airborne soiling measurements of entire solar fields with Qfly, AIP Conf. Proc. 2303 (2020) 100008, https://doi.org/10.1063/5.0028968.
[45] M. Meribout, V. Kumar Tiwari, J. Pablo Peña Herrera, A. Najeeb Mahfoudh Awadh Baobaid, Solar panel inspection techniques and prospects, Measurement 209 (2023) 112466. https://doi.org/10.1016/j.measurement.2023.112466.
[46] H.N. Noura, K. Chahine, J. Bassil, J. Abou Chaaya, O. Salman, Efficient combination of deep learning models for solar panel damage and soiling detection, Measurement 251 (2025) 117185. https://doi.org/10.1016/j.measurement.2025.117185.
[47] G. Picotti, P. Borghesani, G. Manzolini, M.E. Cholette, R. Wang, Development and experimental validation of a physical model for the soiling of mirrors for CSP industry applications, Sol. Energy 173 (2018) 1287–1305, https://doi.org/10.1016/j.solener.2018.08.066.
[48] F. Wolfertstetter, S. Wilbert, F. Terhag, N. Hanrieder, A. Fernandez-García, C. Sansom, P. King, L. Zarzalejo, A. Ghennioui, Modelling the soiling rate: Dependencies on meteorological parameters, AIP Conf. Proc. 2126 (2019) 190018, https://doi.org/10.1063/1.5117715.
[49] F. Wolfertstetter, F. Sutter, E. Lüpfert, M. Montecchi, C. Heras, G. Bern, F. Ise, M. Bitterling, A. Heimsath, F. Ise, A. Fernández-García, J. Wette, A. Asselineau, I. Energy, G. Zhu, Recommendations for reflectance measurements on soiled solar mirrors, (2022).
[50] C. Sansom, A. Fernández-García, P. King, F. Sutter, A. García-Segura, Reflectometer comparison for assessment of back-silvered glass solar mirrors, Sol. Energy 155 (2017) 496–505, https://doi.org/10.1016/j.solener.2017.06.053.
[51] C.B. Anderson, G. Picotti, T. Schmidt, M.E. Cholette, G. Bern, T.A. Steinberg, G. Manzolini, The impact of condensation on solar collector soiling: an experimental study, Sol. Energy Mater. Sol. Cells 275 (2024) 112998, https://doi.org/10.1016/j.solmat.2024.112998.
[52] J.S. Crawford, J. Stewart, J.A. Pérez-Ullivarri, A Comparison of Three Portable Reflectometers for Use in Operations and Maintenance of CSP Plants, in: SolarPACES Conference Proceedings, Marrakech, Morrocco, 2012: p. 10.
[53] M. Montecchi, F. Sutter, Soiling model for spectral reflectance of solar mirrors, Sol. Energy 259 (2023) 356–363, https://doi.org/10.1016/j.solener.2023.05.017.
[54] CSP.guru, A Database of Concentrating Solar Power Plants of the World for Energy Modellers and Analysts. (n.d.). https://csp.guru// (accessed May 1, 2025).
[55] La industria termosolar como motor económico en España, Protermosolar, 2021.
[56] F. Wiesinger, F. Sutter, A. Fernández-García, J. Wette, F. Wolfertstetter, N. Hanrieder, M. Schmücker, R. Pitz-Paal, Sandstorm erosion on solar reflectors: Highly realistic modeling of artificial aging tests based on advanced site assessment, Appl. Energy 268 (2020), https://doi.org/10.1016/j.apenergy.2020.114925.
[57] G. Picotti, M.E. Cholette, C.B. Anderson, T.A. Steinberg, G. Manzolini, Stochastic soiling loss models for heliostats in Concentrating Solar Power plants, Sol. Energy 263 (2023) 111945, https://doi.org/10.1016/j.solener.2023.111945.
[58] R. Pettit, Characterizing solar mirror materials using portable reflectometers, Sandia, Albuquerque, USA, 1982.
[59] N. Martinez, R. Navio, C. Heras, I. Salinas, M. Mainar, A New Portable Specular Reflectometer, Condor: Description, laboratory and field tests., in: Marrakech, Morocco, 2012: p. 9.
[60] S. Öztürk, İ. Küçük, The effect of pigment on the properties of black automotive enamel, (n.d.).
[61] A.R. Hanson, Good Practice Guide for the Measurement of Gloss, National Physical Laboratory, Teddington, UK, 2006.
[62] ISO 2813 - Paint and varnishes - Determination of gloss values at 20°, 60° and 85°, (2014).
[63] S.C.S. Costa, A.S.A.C. Diniz, L.L. Kazmerski, Dust and soiling issues and impacts relating to solar energy systems: Literature review update for 2012–2015, Renew. Sustain. Energy Rev. 63 (2016) 33–61, https://doi.org/10.1016/j.rser.2016.04.059.